Variscan eclogites from the Argentera–Mercantour Massif (External Crystalline Massifs, SW Alps): a dismembered cryptic suture zone

Fabrice Jouffray, Maria Iole Spalla, Jean Marc Lardeaux, Marco Filippi, Gisella Rebay, Michel Corsini, Davide Zanoni, Michele Zucali, Guido Gosso

Variscan eclogites from the Argentera-Mercantour Massif (External Crystalline Massifs, SW Alps): a dismembered cryptic suture zone.

Fabrice Jouffray[a], Maria Iole Spalla[b], Jean Marc Lardeaux[a,c], Marco Filippi[a,b], Gisella Rebay[d], Michel Corsini[a], Davide Zanoni[b], Michele Zucali[b] and Guido Gosso[b]

a UMR 7329 Geoazur, Université Nice Sophia-Antipolis, 250 Rue A. Einstein, Sophia-Antipolis, 06560 Valbonne France.
b Dipartimento di Scienze della Terra ''A. Desio'', Università degli Studi di Milano, via Mangiagalli 34, 20133, Milano Italia.
c Center for Lithospheric Research, Czech Geological Survey, 11821 Praha 1, Czech Republic.
d Dipartimento di Scienze della Terra e dell'Ambiente, Università degli Studi di Pavia, Italia.

Abstract

We document structural, geochemical, petrological and $^{40}Ar/^{39}Ar$ geochronological data performed on Variscan eclogites from the Argentera-Mercantour Massif, southwestern Alps. Based on high-resolution field mapping, we present new eclogite occurrences and discuss the relationships between eclogites and surrounding migmatites. We recognized for the first time preserved eclogite facies assemblages. Trace elements and REE patterns establish that eclogites protoliths are MORBs contaminated by continental crust. Standard thermobarometry and thermodynamic modeling are consistent with P-T values of 640–740°C for 1.5 ± 0.25 GPa, coherent with paleo-geotherms predicted for warm subduction of oceanic crust. We interpret these eclogites as a dismembered cryptic suture zone. $^{40}Ar/^{39}Ar$ dating on amphiboles yields an age of 339.7 ± 12 Ma for eclogite retrogression under amphibolite facies conditions. All these data are combined to link the Argentera-Mercantour Massif in the tectonic framework of both pre-Mesozoic Alpine basement and European southern Variscides.

Keywords: Argentera-Mercantour, southwestern Alps, Variscan eclogites, protoliths geochemistry, metamorphic evolution, $^{40}Ar/^{39}Ar$ dating.

Aknowledgements

We thank Stephen Collett and an anonymous reviewer for their generous, thoughtful and detailed comments on an early version of this manuscript.

Italian authors acknowledge funding by PSR2019-IBOLLATI (University of Milano). We thank Pavla Štípská for her editorial work.

Introduction

High pressure (HP) metamorphic rocks exposed in mountain belts provide first-order constraints for addressing evolution of orogens (Ernst and Liou 2008) and mafic eclogites are of particular interest because they are records of old subduction zones (Miyashiro 1961; Ernst 1971). In the European Variscan belt, HP metamorphic rocks are widespread (Medaris et al. 1995; Ballèvre et al. 2009; Schulmann et al. 2009; Martínez Catalán et al. 2009; Lardeaux et al. 2014) and have been extensively considered to provide information on pre-continental collision plate tectonics framework (Matte, 2001; Schulmann et al. 2005, 2014; Franke et al. 2017).

Mafic eclogites are also exposed in Variscan basement slices preserved in the Alpine belt (Fig. 1 and "Online Resource 10"; Spalla and Marotta 2007; Spalla et al. 2014; Roda et al. 2019 with references therein). In the External Crystalline Massifs (ECMs) of the western Alps, eclogites that retain protolith geochemical signature and pre-alpine HP mineralogy are rare (von Raumer 1984; Latouche and Bogdanoff 1987; Bogdanoff et al. 1991; Ferrando et al. 2008; Rubatto et al. 2010). The Argentera-Mercantour Massif (Fig. 1) is the southernmost of the ECMs, within which the metamorphic evolution of mafic eclogites remains poorly constrained. We document here the discovery of preserved omphacite (jadeite contents up to 42 mol%) within the retrogressed eclogites of this Massif. Our goal is to present and discuss structural, geochemical, mineralogical, petrological and $^{40}Ar/^{39}Ar$ geochronological data on these Variscan HP metamorphic rocks.

Geological setting

The ECMs belong to the Helvetic-Dauphinois domain of the Alpine belt (Schmid et al. 2004), where Alpine tectonic history has not significantly erased Variscan signatures (Von Raumer et al. 1999, 2009, 2013; Guillot and Menot 2009; Compagnoni et al. 2010; Spalla et al. 2014; Fréville et al. 2018). The Argentera-Mercantour Massif, located at the French-Italian border, is a piece of European continental crust shortened in response to late Alpine collision (Polino et al. 1990; Bogdanoff et al. 2000; Schwartz et al. 2007; Schreiber et al. 2010).

Following the first investigations of Faure-Muret (1955), Malaroda and Schiavinato (1958, 1960) and Malaroda et al. (1970), this massif was systematically divided into two main units (Bogdanoff et al. 1991; Rubatto et al. 2001; Compagnoni et al. 2010; Carosi et al. 2016) separated by a steeply dipping, NW-SE striking, km-scale shear zone, the « Ferriere-Mollières Shear Zone » (FMSZ, Fig. 2), also known as « Valletta Shear Zone ». The FMSZ, recognized since Faure-Muret (1955), is a dextral transpressive shear zone active in Late Carboniferous

times (i.e. 330–310 Ma, Musumeci and Colombo 2002; Corsini et al. 2004; Simonetti et al. 2018) and significantly re-activated during Alpine times (i.e. 27–21 Ma, Corsini et al. 2004; Sanchez et al. 2011). HP/HT metamorphic rocks are described in the western and eastern complexes (Faure-Muret 1955; Malaroda et al. 1970), which consist of Variscan high-grade migmatites derived from meta-sediments (Bortolami and Sacchi 1968; Blasi 1971; Malaroda et al. 1970) or from meta-granitoids (Bogdanoff and Ploquin 1980; Bogdanoff et al. 1991). Upper Ordovician to Lower Silurian ages have been obtained for magmatic protoliths (Rubatto et al. 2001).

The main pre-Alpine structure is a pervasive steeply dipping regional-scale foliation defined by a shape preferred orientation of biotite, feldspar and sillimanite, and by alternating quartz + feldspars + biotite ± garnet-bearing leucosomes and biotite-rich melanosomes.

In the eastern unit post-kinematic cordierite-bearing leucocratic diatexites are widespread (Blasi and Schiavinato 1968). At the regional scale, coarse-grained undeformed cordierite-bearing melts clearly crosscut the main foliation. In both complexes centimeter-scale cordierite-rich leucosomes intersect and progressively erase the main foliation in biotite and sillimanite-bearing migmatites. Two main partial melting events can be inferred: the first syntectonic episode (M1) developed in equilibrium with biotite, garnet and sillimanite, and the second (M2), clearly post kinematic, in equilibrium with cordierite, at lower pressure. The age of 323 ± 12 Ma obtained by U/Pb on zircons dates the last regional migmatitic event (Rubatto et al. 2001).

Within the eastern complex, a large granitic stock (Fig. 2) intersects the foliation (Boucarut 1967; Ferrara and Malaroda 1969). This granite is dated at 292 ± 10 Ma by Ferrara and Malaroda (1969) and in the range 299–296 Ma by Corsini et al. (2004), and belongs to the late Carboniferous Fe-rich granitoids (Debon and Lemmet 1999) in the EMCs of the western Alps.

The exhumation of the Argentera-Mercantour Variscan crust is sealed by impure sandstones and black shales, rich in upper Pennsylvanian vegetal fossils, filling intra-mountain basins bordered by strike-slip faults (Corsin and Faure-Muret 1946, 1951; Faure-Muret and Fallot 1955).

During Alpine collision the Argentera-Mercantour Massif was metamorphosed under upper greenschist facies conditions (Corsini et al. 2004; Lardeaux 2014a; Filippi et al. 2019). Alpine deformation is concentrated in ductile shear zones marked by alternating fine grained recrystallized quartz + albite and muscovite + chlorite ± titanite-rich layers (Sanchez et al. 2010, 2011).

Eclogites in the Argentera-Mercantour Massif: Localized or diffuse occurences?

In the Ibero-Armorican arc and French Massif Central, mafic eclogites are localized in specific horizons (Leptyno-Amphibolite Complexes) in association with ultramafic rocks and HP felsic rocks (Martínez Catalán et al. 2007; Ballèvre et al. 2009; Faure et al. 2009; Lardeaux 2014b). These horizons are localized at the base of the allochtonous nappes thrusted upon low-pressure units (Matte and Burg 1981; Ledru et al. 1989, 2001; Lardeaux et al. 2001; Berger et al. 2010). In Sardinia or Maures-Tanneron Massif (southern European Variscides) eclogites are recognized as lenses dispersed within migmatites (Carmignani et al. 1994; Franceschelli et al. 2007; Cruciani et al. 2011; Schneider et al. 2014).

In the Argentera-Mercantour Massif, the presence of rare eclogites was first reported by Faure-Muret (1955) and other limited occurences identified later (Malaroda et al. 1970; Latouche and Bogdanoff 1987; Colombo et al. 1994; Rubatto et al. 2001). Ages of 459 ± 4 Ma and 486 ± 7 Ma have been obtained by U-Pb dating on zircons for protoliths of HP mafic rocks (Rubatto et al. 2001, 2010). We discovered a significant number of other occurrences (Fig. 2) with specific characters: First, eclogites occur as poorly deformed lenses, centimetric to metric thick, within surrounding migmatites (Fig. 3). Second, boudins of eclogites can be associated with mafic HP granulites and/or serpentinites. Up to now, an association with HP felsic granulites remains unknown. Third, eclogites are severely retrogressed under amphibolite facies conditions: preserved eclogite facies assemblages are exceptional (Fig. 4). Last, eclogites occur in both western and eastern units in all types of migmatites, i.e. within biotite-sillimanite-garnet banded M1 migmatites as well as within leucocratic cordierite bearing M2 migmatites, but also within migmatitic orthogneisses and migmatitic amphibolites.

Typical field relationships are illustrated by two lithological and structural maps (Figs. 5 and 6).

In this massif, mafic granulites have been studied in detail (Ferrando et al. 2008; Rubatto et al. 2001, 2010), but petrological and structural analyses on eclogites remain scarce, probably because deciphering preserved eclogite facies assemblages is rare.

Geochemistry of eclogites

Analytical conditions and results are given in “Online Resource 1”.

Major elements

Our samples, displaying mid ocean ridge basalt (N-MORB) average composition (McKenzie and O'Nions 1991), show a weak depletion in CaO and TiO_2 and an enrichment in K_2O. On the Al_2O_3 vs. TiO_2 diagram (Konzett et al. 2012), they tend to lie in the basalt field and for a few samples in plagioclase-rich cumulates (Fig. 7), suggesting that their protoliths were basalts and gabbros.

In the Total Alkali versus Silica diagram (Online Resource 2) SiO_2 content ranges from 40.51 to 52.01 wt% and our sample compositions are mainly in the field of basalts, while in the AFM diagram, they plot mainly in the fields of tholeiitic, and for a restricted number of samples in the calc-alkaline volcanic series (Fig. 7).

However, major elements are mobile during metamorphism (Winchester and Floyd 1977). Taking into account that surrounding migmatites have undergone dehydration reactions coeval with retrogression of eclogites, the latter could have experienced chemical contamination from outside (see Štípská et al. 2014 for example). Consequently K_2O enrichment from surrounding migmatites is possible. We therefore consider the least mobile elements during alteration and metamorphism (i.e. HFS elements such as Sc, Y, Zr, Hf, Ti, Nb and Ta, or REEs) when using chemical diagrams for protoliths characterization.

Trace elements and REE

The eclogites have typical N-MORB compositions in the Zr-Ti-Nb-Y (Pearce 1996) or in the Y-Nb-Zr (Meschede 1986) diagrams, except for two samples displaying within-plate chemical signatures and corresponding to a foidite and a picrobasalt (Fig. 8a, see also Online Resource 2).

In discriminant diagrams (Fig. 8b, and Online Resources 3,4 and 5) sample compositions plot in the field of tholeitic basalt and MORB, whereas a few of them show affinity with calk-alkaline to alkaline basalts. This can be interpreted as the consequence of various tectonic contexts of protoliths formation or as the result of chemical contamination during protoliths formation and/or evolution. To face these uncertainties, the best tools are the diagrams proposed by Pearce (2008) or the chondrite normalized Th vs. Nb (normalization according to Sun and McDonough 1989) proposed by Saccani (2015), within which the effects of crustal contamination on fractional crystallization and on the MORB-OIB array can be depicted. In these diagrams, a significant number of our samples plot outside the MORB-OIB array suggesting that these rocks have been contaminated by crustal components (Fig. 8c, see also Online Resource 6).

158 The Nb/La ratio is regarded as an index of crustal contamination of magmas (Thompson et al. 1983). For our
159 eclogites, this ratio ranges between 0.20 and 1.71 with a mean value of 0.7. For comparison, MORB and OIB
160 typically show values of 0.93 and 1.3 respectively (Sun and McDonough 1989), while continental flood basalts
161 display values of 0.14–1.4 (Thompson et al. 1983). This indicates that our samples have undergone crustal
162 contamination.
163 Contamination is also suggested by low and variable Zr/Hf ratios (mean value of 34.11) and Nb/Ta ratios (mean
164 value of 12.47) in comparison with those of N- and E-MORB (respectively 36 and 17 according to Sun and
165 McDonough 1989). Moreover, MORB and OIB have uniform value of 25 ± 5 for their Ce/Pb ratio whereas the
166 mean value for continental crust is around 4 (Hofmann et al. 1986). The Ce/Pb value of our samples is in the
167 range of 0.03-15.7 (with a mean value of 5.12) and thus compatible with crustal contamination of MORB
168 basalts.
169 According to Hofmann (2003), the Nb/U and the Pb/Nd ratios are indicators for crustal contamination. Nb/U
170 ratio of 47 ± 11 is typical for MORBs, while the mean value of continental crust is 8 (Rudnick and Fountain
171 1995). This ratio varies from 2 to 47.8 with a mean value of 12.6 for the studied eclogites. The Pb/Nd ratios are
172 of 0.04, 0.07, 0.08, and 0.63 for N-MORB, E-MORB, OIB, and continental crust respectively (Hofmann 2003).
173 Our eclogites present a Pb/Nd ratio ranging between 0.14 and 1.81 with a mean value of 0.41. This confirms
174 crustal contamination.
175 The total REE content indicates that most samples show an enrichment, 10–40 times greater than average N-
176 MORB. The REE patterns of the Argentera-Mercantour eclogites are presented in Fig. 9 and the patterns of OIB,
177 N-MORB and E-MORB are shown for comparison.
178 Primitive mantle normalized trace element pattern shows contrasting trends: a first group of samples show
179 enrichment in LREE with respect to HREE, whereas the second is characterized by slightly depletion,
180 compatible with E-MORB and N-MORB trends, respectively. Some samples are characterized by strong Th
181 depletion, similar to average N-MORB values, whereas a few others have Th positive anomaly. All samples
182 show positive Rb, Pb and U anomalies and trends with Sr and Ba depletions, and most of them Nb, Ta and Mo
183 depletions. These trends are relevant markers for contaminated basaltic sources (Donnelly et al. 2004). Finally,
184 the $(La/Sm)_N$ ratio is highly variable (0.42-3.09), indicating various degrees of fractionation (Carlson 2003) .
185
186
187

Petrography of eclogites

The Argentera-Mercantour eclogites experienced severe retrogression and eclogite facies assemblage is rarely preserved. The cores of the boudins consist of fine-grained rocks with reddish millimeter to centimeter-sized garnets but their margins are totally transformed into garnet-free amphibolites.

The peculiar features of these eclogites are the occurrence of clinopyroxene-plagioclase symplectitic domains and of plagioclase-brown/green amphibole symplectitic coronas around garnets (Fig. 10a, b, c, d and f). The development of clinopyroxene-plagioclase symplectites results from omphacite destabilization and is a discontinuous precipitation explained in terms of decreasing pressure with or without temperature increase (Boland and Van Roermund 1983; Joanny et al. 1989, 1991). Some of our samples show an evolution of the symplectite texture, with thinner clinopyroxene lamellae developed at the expense of the coarser ones (Fig. 10b).

Garnet occurs as grains up to 5 millimeter in size containing inclusions of quartz, amphibole, rutile, zircon and in some samples small sized brown biotite, epidote, ilmenite, apatite and monazite (Fig. 10e). In one sample (Lac Niré), an inclusion of omphacite, associated with amphibole, was observed within garnet.

Amphibole, the most abundant phase, occurs in different textural sites: inclusions within garnets, large green to light-brown amphibole grains in the matrix, brown amphibole rims near the plagioclase-clinopyroxene symplectites, discontinuous droplets in association with plagioclase within coronas around garnets, large poikiloblastic green-brown grains, in association with biotite, fully replacing the symplectites or invading totally the garnets grains, and pale green amphibole filling late veins.

Plagioclase occurs together with clinopyroxene in symplectites replacing omphacite, but also together with the dark-brown amphibole rimming garnet or amphibole 1, close to the symplectites or together with droplets of amphibole around garnet, and in late veins associated with titanite, chlorite, white mica, biotite and pale green amphibole.

In the matrix, rutile grains are usually rimmed by ilmenite. Quartz is common and biotite and K-feldspar are interstitial with respect to garnet, clinopyroxene and amphibole 1 and 2. In the most retrogressed samples, chlorite is developed at the expense of biotite and amphibole as well as in the fractures of garnet.

Mineral chemistry

Mineral analyses were performed on 3 samples (Lac Long, Lac Niré and Pas des Ladres) in the French part of the massif, and 3 samples (upper Valasco Valley) in the Italian part. Analytical conditions and results are presented in "Online Resource 7".

Garnet from French samples is almandine-rich (almandine 49–56 mol%) and spessartine-poor with pyrope, grossular contents ranging from 20 to 32 and 17 to 24 mol% respectively. In the diagram of Coleman et al. (1965), garnets are distributed between the fields of B and C eclogite types (Fig. 11b). The zoning pattern is limited to the mineral rims, with an increase in almandine content correlated to a decrease of pyrope and grossular contents.

In Valasco Valley, garnet is Fe-rich (almandine 61–54 mol%) with low spessartine (3–6 mol% at core, 1–3 mol% at rim), pyrope and grossular contents 8–12 mol% and 21–32 mol%, respectively. They plot in the field of type C eclogites (Fig. 11b) showing a constant pyrope content and grossular enrichment from core to rim. Indeed Mn and Fe^{2+} decrease from 0.16 to 0.01 and 1.83 to 1.70 apfu, respectively, whereas Ca slightly increases from 0.75 to 0.96 apfu, from core to rim.

Clinopyroxene was identified in different sites. In the Lac Niré sample, the clinopyroxene inclusion within garnet is omphacite with jadeite content around 32 mol%. In Lac Niré as well as in Pas des Ladres eclogites, clinopyroxene 1 is replaced by clinopyroxene 2 + plagioclase symplectites. In the coarser lamellas, the jadeite component is 42 mol%, while the thinner ones have jadeite contents of 15–27 mol% (Fig. 11a).

In Valasco Valley, clinopyroxene 1 is not preserved, but its composition has been estimated, by mass balance calculations of symplectite domains, at a jadeite content from 24 to 38 mol%. Pyroxene in symplectite (Cpx 2) is always diopside with jadeite content < 5 mol% in all localities.

Plagioclase lamellae from the symplectites are oligoclase (anorthite 20–32), while plagioclase forming coronitic shells around garnet in equilibrium with amphiboles is andesine (Fig. 11c). Plagioclase in veins with actinolite is anorthite 8–13.

Amphiboles, from Pas des Ladres and Lac Niré are calcic (Fig. 11d) according to the classification of Leake et al. (2004) and Hawthorne et al. (2012). The amphiboles in inclusions within garnets are magnesio-hornblendes with Mg content of about 0.22 to 0.31 apfu. The amphiboles from coronas around garnet and the amphiboles replacing clinopyroxene of the symplectites, or invading garnets are magnesio-hornblendes with Mg content of about 0.30 to 0.38 apfu.

In Valasco Valley, amphibole 1 and 2 are mostly pargasite. Amphibole 3a is ferro-pargasite, amphibole 3b is mostly ferro-edenite or magnesio-hornblende. Amphibole 4 is actinolite. Amphibole 1 and 2 have Al^{IV} between 1.53–2.04 apfu and Al^{VI} between 0.37 and 0.74 apfu. Ti content in amphibole 1 varies between 0.12 and 0.20 whereas amphibole 2 is Ti-richer (from 0.20 to 0.31 apfu). Na content decreases from 0.55 apfu in amphibole 1 to 0.49 apfu in amphibole 2.

Amphibole 3a, in rims around garnet, is particularly Al-rich (Al_{tot} from 2.55 to 3.74 apfu, clustering at 3.06 apfu), with XMg < 0.5 and Ti lower than 0.14 apfu. Amphibole 3b, mainly replacing clinopyroxene, has Al_{tot} between 0.75 and 2.07 apfu and Ti lower than 0.07 apfu. Amphibole 4 has Al_{tot} <0.70 apfu and Ti< 0.04 apfu everywhere.

Metamorphic history and P-T evolution

The Argentera-Mercantour eclogites preserve evidences of a first eclogitic stage documented by the occurrence of almandine-rich garnet and by the preservation of omphacite (jadeite 42 mol%) within symplectites and as inclusion within garnet (jadeite 32 mol%). Mineral inclusions in garnet suggest that the stable mineral assemblage during this stage was garnet + omphacite + calcic amphibole + quartz + rutile + zircon ± epidote ± biotite.

A post-eclogitic stage is evidenced by the development of clinopyroxene (jadeite 27-5 mol%)-plagioclase symplectites at the expense of omphacites and plagioclase-calcic amphibole-ilmenite coronas around garnets. Rutile is replaced by ilmenite in the matrix. Garnet rims are in equilibrium with amphibole-plagioclase coronas containaing in some samples also diopside. This last assemblage is typical for granulite-facies conditions.

An amphibolite-facies stage is constrained by the replacement of symplectitic clinopyroxenes by amphiboles and the development of poikiloblastic amphiboles, in association with biotites and ilmenite, at the expense of all previous minerals.

A late stage is documented by formation of micro-cracks filled with albite, actinolite, titanite and chlorite and by replacement of biotites and calcic amphiboles by chlorite. The replacement of ilmenite by titanite can also be related to this late stage (greenschist facies conditions).

A first approach for estimation of eclogitic P-T conditions is the use of experimentally determined domains for the observed mineralogy. For samples with chemical compositions of N-MORB, we use the grid determined by Schmidt and Poli (1998). With H_2O in excess, the association garnet-omphacite-amphibole-quartz is stable in the

range 600–700°C for 1.4–2.4 GPa. This estimation is in agreement with the field of amphibole bearing eclogite facies for basaltic compositions (Ernst and Liou 2008)

Thermobarometry is a second approach and Fe^{2+}-Mg exchange between garnet and clinopyroxene is well adapted for eclogites. The calibration established by Krogh-Ravna (2000) integrates the effects of Ca and Mn components and requires clinopyroxene with a sodic content in the range 0–0.51 to work. Because of severe retrogression, this thermometer was only applied in the Lac Niré sample using the preserved inclusion of omphacite (Na content of 0.33) within garnet. Application of this geothermometer, for pressure from 1.2 to 1.4 GPa, showed temperatures of 710 - 720°C.

The garnet–hornblende Fe-Mg thermometer (Graham and Powell 1984), applied to Lac Long samples showing inclusions of magnesio-hornblende with rational grain boundaries with garnet and in equilibrium with quartz and rutile, gives a range of 640–690 °C.

However, the reliability of Fe-Mg exchange thermometry is dependent on uncertainties in estimation of the Fe^{3+}/Fe^{tot} ratios in minerals (Carswell et al. 2000). As established by Štípská and Powell (2005), if Fe^{3+} content is not taken into account for garnet-clinopyroxene thermometry the calculated temperatures are overestimated, therefore the proposed values (710–720°C) are considered as maximum temperatures.

We used also the Zr-in-rutile thermometry (Watson et al. 2006, Thomkins et al. 2007) relevant for quartz and zircon-bearing rocks. In the Lac Niré eclogite, the Zr content in rutiles in inclusion within eclogitic garnet is between 221 and 458 ppm. Application of the Zr content in rutile thermometer for pressure of 1.2 and 1.5 GPa showed temperatures of 634–694 and 646–706°C respectively.

The minimal pressure of the eclogitic stage is estimated at 1.4–1.6 GPa using the maximal values of the jadeite content (32–42 mol%) of omphacites (Gasparik and Lindsley 1980; Holland 1990).

Ti-content in amphibole thermometer (Otten 1984), using the core compositions of in amphibole 1 grains, gives temperatures of 680–715°C in Valasco Valley eclogites. Ernst and Liu (1998) calibration suggests T= 700–740°C, using the same data, for which Al-content indicates P = 1.1–1.7 GPa.

In summary, application of various thermo-barometers, to all the studied samples, yields to a P-T range of 640–740°C and 1.1–1.7 GPa (Online Resource 8).

Thermodynamic calculations were performed with the free energy minimization program THERIAK/DOMINO (De Capitani and Petrakakis 2010, version 2015). Pseudosections were calculated for two samples from Valasco Valley and Lac Long (Fig. 12). Compositions were chosen starting from the whole rock analysis, considering H_2O in excess, and not considering the presence of a melt, as the mafic boudins are enclosed in migmatitic felsic

rock, but without evidence of internal melting. For Valasco Valley, we have removed K_2O from the composition, as biotite and K-feldspar occur as interstitial grains or filling late veinlets suggesting that boudins were contaminated during country rocks partial melting. For Lac Long sample, because biotite was observed in equilibrium with eclogitic garnet, K_2O was considered in the system. Finally, we have evaluated the effect of O and H_2O on our pseudosection, as suggested by Guiraud et al. (2001) and Rebay et al. (2010) to evaluate their effect on the stability and preservation of assemblages. We used the following mineral a-x relations: plagioclase (Holland & Powell 2003), garnet (White et al. 2007), ilmenite (White et al. 2000), amphibole (Diener et al. 2007), clinopyroxene (Green et al. 2007), orthopyroxene (White et al. 2002), biotite, (White et al. 2007) and white mica (Coggon and Holland 2002). The thermodynamic database is ds55 (Holland and Powell 1998).

Valasco Valley pseudosection is represented in Fig. 12a where the observed assemblage garnet, amphibole 1, omphacite, rutile and quartz, is stable in a field that spans from 625 to 740 °C and 1.2 to 1.75 GPa. This penta-variant field is limited by the appearance of plagioclase towards high temperatures, the disappearence of amphibole towards higher pressure and temperatures, the appearance of a jadeitic pyroxene at higher pressures and lower temperatures, the presence of clinozoisite at lower temperatures and the presence of titanite towards lower temperatures. The compositions of clinopyroxene and amphibole in the field are close to those detected in Valasco Valley eclogites. In addition thermobarometric estimates performed on eclogite facies minerals from Valasco Valley rocks perfectly fit with the HP assemblage stability field. Addition of Fe_2O_3 would shift epidote stability towards higher temperature, up to close the penta-variant field we are interested in for around 10 mol% of FeO_t as F_2O_3. Conversely, plagioclase-in and amphibole-out lines would be affected only by minor shifting towards higher temperatures and pressures, respectively, of the order of four tens of Celsius degrees and less than 0.1 GPa. A similar configuration would result from taking into account zoisite instead of clinozoisite in a Fe_2O_3-free system.

In the Lac Long pseudosection (Fig. 12b) the assemblage amphibole, omphacite, garnet, rutile, quartz and biotite is stable in a P-T range of 600 to 780°C and 1.25 to 1.80 GPa, in agreement with thermobarometric estimates. The proposed field is bounded by plagioclase at high temperature, amphibole at high pressure, phengite at low temperature, and titanite and clinozoisite at low pressure. If we consider zoisite instead of clinozoisite, the lower temperatures field boundary would be shifted to T at around 690°C, still in agreement with other P-T determinations made for this assemblage. Addition of Fe_2O_3 would shift both epidote stability towards higher temperature, and phengite towards higher temperature and lower pressure, until the closing of the penta-variant

field of interest for slightly more than 10 mol% of FeO_t as Fe_2O_3. The effects on the other field boundaries are negligible.

Geochronological constraints on eclogite facies metamorphism

Ages of eclogite facies metamorphism previously obtained in the eclogites from the ECMs, as well as from other segments of the European Variscan belt, are not well constrained (Von Raumer et al. 2009; Paquette et al. 2017, Lotout et al. 2018). The geochemical signatures of the studied eclogites are totally consistent, particularly regarding multi-elements abundance patterns, with those obtained for HP mafic granulites sampled in the Argentera-Mercantour Massif (Rubatto et al. 2001, 2010) suggesting that these HP mafic granulites could be considered as markers of the incipient stage of eclogites retrogression. In such a case the age of eclogite facies metamorphism is probably close to that obtained for HP granulite facies, i.e. 340 ± 4 Ma (Rubatto et al. 2010) by U/Pb zircon dating. So far, we have not enough zircons from eclogites to try to get an age of the eclogite facies metamorphism. However, we performed $^{40}Ar/^{39}Ar$ dating on amphiboles from these eclogites. We selected a sample from the Lac Long eclogites. This sample (LL09-12J) is closely associated with the (LL13) sample used for the previously presented pseudosection and has a similar geochemistry. In this (LL09-12J) sample, magnesio-hornblendes are in textural equilibrium with plagioclase, ilmenite and garnet. The inferred age corresponds thus to the re-equilibration of eclogites under amphibolite facies conditions.

Analytical conditions and results are available as "Online Resource 9". Amphibole single grain of Lac Long sample (LL09-12J) yields a plateau age (Fig. 13) at 339.7 ± 12 Ma corresponding to 93.77 % Ar released and to four steps. The inverse isochron for the plateau steps gives a concordant age at 339.8 ± 12 Ma (MSWD = 2.17). The plateau-age at 339.7 ± 12 Ma is considered as the best age estimate for the record of amphibolite facies imprint.

Discussion and conclusions

Origin of eclogites protoliths

Trace elements and REE patterns establish that the Argentera-Mercantour eclogites are MORBs contaminated by continental crust components. Crustal contamination can be the consequence of contamination of basaltic

liquids, i.e. eclogite protoliths, prior to HP metamorphism or contamination of eclogites by surrounding migmatites during or after their emplacement.

In the first hypothesis, the multi-element diagrams of incompatible elements display Pb, U and Large Ion Lithophile Element (LILE) enrichments, and also Nb and Ta depletions. These patterns are characterisric of arc lavas and back-arc basalts (Hofmann 2003; Labanieh et al. 2012). In that case, the geochemical signatures of the studied eclogites are more compatible with those of supra-subduction zone basalts rather than those oceanic domains.

Considering the second hypothesis, during high temperature hydrothermalism as well as during high-temperature crustal melting, significant K, Pb, U and more generally LILEs influxes by crust-derived fluids migration can be envisaged (Michard and Albarède 1986; Pattison 1991; Klinkhammer et al. 1994; Štípská et al. 2014). In such a case, the eclogite protoliths could be standard MORBs later contaminated during orogenic processes.

Paleo-gradient and context for eclogites formation

The eclogite-facies conditions were quantified by independent methods as comparison between natural and experimentally determined mineral assemblages, well calibrated independent thermobarometers and thermodynamic modeling. The obtained results are consistent with temperatures comprised between 640 and 740°C for pressure of 1.5 ± 0.25 GPa.

To infer their geodynamic significance, we compare these P-T estimates with metamorphic gradients (Miyashiro 1961; Ernst 1971; Spear 1993) and with geotherms proposed by Cloos (1993) for cold and warm subductions (Fig. 14).

The eclogitic stage fits the conditions predicted by the the different models calculated for warm subduction of oceanic crust and therefore they represent the traces of a suture zone.

The Argentera-Mercantour Massif: record of a dismembered suture zone

The Argentera-Mercantour eclogites are witnesses of an oceanic crust formed in a back-arc basin or in an oceanic domain. Whatever is the selected pre-orogenic configuration, these rocks are the exhumed remnants of subducted oceanic crust, therefore localizing a paleo-suture zone transposed after continental collision in a migmatitic complex. However this paleo-suture zone is totally dismembered and eclogites are mixed with

various types of migmatites. The original suture is totally overprinted by mass transfer of partially molten continental crust, giving rise to a "diffuse cryptic suture zone" in the sense of Schulmann et al. (2014).

The mechanism leading the extensive dismembering of the suture zone remains unclear and different models can be considered. We can envisage dismembering, during continental collision, of previously stacked ophiolitic unit in response to vertical transfer (i.e. extrusion) of hot partially molten orogenic crust during ongoing shortening. This results in large–scale gravity driven migmatitic dome-like structures favouring mixing of eclogites and migmatites as proposed in Variscan Bohemian Massif (Štípská et al. 2004; Schulmann et al. 2005, 2009, 2014) or in the Maures-Tanneron Massif (Schneider et al. 2014, Gerbault et al. 2018). We can also consider dismembering of subducted crust during oceanic subduction and/or incipient collision leading the formation of a "hot subduction channel" composed of subducted, partially molten, upper crustal rocks and lithospheric hydrated mantle rocks as proposed by et al. (2008). The result is a " hot subduction mélange", localized at the plates interface, producing fast exhumation of mafic HP rocks within molten meta-sediments.

The Argentera-Mercantour eclogites in the southern European Variscides framework

Considering field relationships between eclogites and surrounding migmatites, their geochemistry, and petrological evolutions, the Argentera-Mercantour eclogites show remarkable similarities with Sardinian eclogites (Giacomini et al. 2005; Franceschelli et al. 2007; Cruciani et al. 2015, 2017; Fig. 14), with eclogites from the Maures-Tanneron Massif (Bard and Caruba 1982; Briand et al. 2002; Corsini and Rolland 2009; Schneider et al. 2014) and finally with Corsican eclogites (Palagi et al. 1985; Lardeaux et al. 1994; Faure et al. 2014).

The European Variscan belt is the result of tectonic accretion of Gondwana derived micro-plates colliding with Laurussia during the Devonian (Torsvik et al. 1990, 1996; Tait et al. 1997; Matte 2001;Von Raumer et al. 2002; Cocks and Torsvik 2011; Stampfli et al. 2013). The continuity of this process led to the formation of a huge collision belt and to the amalgamation of the Pangea supercontinent in the late Paleozoic (Franke 1989, 2000; Matte et al. 1990; McKerrow et al. 2000; Domeir and Torsvik 2014). Among the various micro-plates involved in this evolution, paleomagnetic constraints combined with geochronological data and regional geologic investigations have identified, in the southern Variscides, the so-called Maures-Esterel-Corsica-Sardinia ("MECS") block (see Edel et al. 2014, 2018). If we consider that the occurrences and the petrochemical characteristics of eclogites are critical for deciphering the main suture zones in orogenic systems, the similarities

between HP metamorphic rocks recognized in Argentera-Mercantour, Sardinia, Maures-Tanneron and Corsica suggest that the southernmost ECMs possibly linked with the MECS block. Such a link is also consistent with various paleo-plates tectonic reconstructions proposed by Stampfli et al. (2013). In the framework of Gondwana derived micro-plates these authors distinguish, during upper Devonian times, northern blocks (Iberian Massif, Armorican Massif, French Massif Central, Bohemian Massif), located close to the Rheic (or Rheno-Hercynian) ocean and southern blocks (Sardinia, Corsica, ECMs,…) located close to the Paleo-Tethys. In such a scheme, the ages of eclogite facies metamorphism are different with a decrease of geological ages of HP metamorphism from northern to southern blocks. Geochronological data are therefore first-order constraints to discuss these models.

In the MECS block, late Cambrian-Ordovician to lower Silurian protolith ages of HP rocks are constrained by U/Pb zircon dating (Innocent et al., 2003; Palmeri et al. 2004; Giacomini et al. 2005, 2008; Rossi et al. 2009; Schneider et al. 2014; Cruciani et al. 2017). This time span is coherent with ages of 459 ± 4 Ma and 486 ± 7 Ma obtained in the Argentera-Mercantour Massif (Rubatto et al. 2001, 2010) but also with as all protoliths ages obtained in the ECMs (Von Raumer et al. 2002; Schultz et al. 2004). In the MECS block, the timing of crustal anatexis is constrained in the range 345-310 Ma (Di Vicenzo et al. 2004; Giacomini et al. 2005, 2008; Demoux et al. 2008; Rossi et al. 2009; Corsini et al. 2010; Faure et al. 2014; Li et al. 2014; Cruciani et al. 2015; Oliot et al. 2015). The age of 323 ± 12 Ma obtained for crustal partial melting in the Argentera-Mercantour Massif (Rubatto et al. 2001) as well as our age at 339.7 ± 12 Ma for eclogite re-quilibration under amphibolite facies conditions are in agreement with these results. A characteristic signature of continental collision in the MECS block is the development of a transpressive regime in the range 330-310 Ma leading the development of ductile strike-slip shear zones in Sardinia (Elter et al. 1990; Carosi and Oggiano 2002; Carosi et al. 2004, 2009) and Maures-Tanneron Massif (Corsini and Rolland 2009; Corsini et al. 2010). In the Argentera-Mercantour Massif, the FMSZ transpressive shear zone active in the range 330-310 Ma (Simonetti et al. 2018) is a record of a similar tectonic regime.

However, the ages of eclogite facies metamorphism remains poorly constrained in the MECS block as well as in the ECMs (Von Raumer et al. 2009; Schneider et al. 2014; Cruciani et al. 2015; Spalla et al. 2014; Regorda et al. 2019) and new radiometric datings are necessary to discriminate between the different geodynamic scenarios. The U/Pb zircon age obtained on HP granulites in Corsica at ca. 360 Ma is still debated (Li et al. 2014), therefore the only available geochronological constraints are the age of HP mafic granulites at ca. 340 ± 4 Ma (Rubatto et al. 2010) and the the time span of 344-330 Ma. for retrogression of eclogites under amphibolite facies.

In the framework of the Alpine belt, the identification of which and how many Variscan suture zones (e.g. Matte 1986, 2001; Franke 2000; Faure et al. 2005; Guillot et al. 2009; Lardeaux et al. 2014) occur in the Alpine chain is still debated (Regorda et al. 2019). The evolution of this Palaeozoic lithosphere in terms of geodynamic scenario has been rarely explored (e.g. von Raumer et al. 2003, 2013; Spiess et al. 2010). The discussion on the provenance of the Alpine basement units in terms of palaeogeography and influence of Palaeo-Tethys evolution on the Variscan dynamics is still open. For this purpose, the comparison of the thermo-mechanical evolution of the Argentera-Mercantour eclogites with those of other Variscan eclogites from the Alps is a key starting point to shed light on their geodynamic significance (Fig. 14 and "Online Resource 10"). PT conditions inferred from eclogites and HP-granulites of Helvetic Domain indicate a thermal state higher than that of warm subduction zones (Cloos 1993), mainly compatible with the initial unperturbed geotherm or higher, with the only exception of Valasco Valley and Lac Niré rocks. The P-T conditions of the latter lie on the warm subduction geotherm, fully comprised in the Franciscan metamorphic gradient, like some of the Sardinian eclogites. For the first time this indicate that oceanic subduction-related metamorphism developed also in the Helvetic Variscan crust. This makes the investigated rocks more similar to the Variscan eclogites from other Alpine structural domains, which mainly show a thermal state between warm and cold subduction gradients or locally colder, as the case of some Austroalpine eclogites from Oetztal, Tonale and Silvretta nappes.

The previously presented constraints demonstrate the coherence of the Variscan geological signatures depicted in the Argentera-Mercantour Massif and those of the MECS block, which share the same tectono-metamorphic evolution. Hence we envisage that the southernmost ECM is a part of the MECS block in the framework of the European Variscan belt. To test such a hypothesis it will be now critical to obtain high-resolution chronological constraints on the age of eclogite facies metamorphism, particularly in Argentera-Mercantour and Maures-Tanneron Massifs.

References

Ballèvre M, Bosse V, Ducassou C, Pitra P (2009) Palaeozoic history of the Armorican Massif: models for the tectonic evolution of the suture zones. C R Geoscience 341:174–201.

Bard JP, Caruba C (1982) Texture et minéralogie d'une éclogite à disthène-saphirine-hypersténe-quartz en inclusion dans les gneiss migmatitites des Cavaliéres, massif de Ste Maxime (Maures, Var, France). C R Acad Sci Paris 294:103–106.

Berger J, Féménias O, Ohnenstetter D, Bruguier O, Plissart G, Mercier JC, Demaiffe D (2010) New occurrence of UHP eclogites in Limousin (French Massif Central): age, tectonic setting and fluid–rock interactions.

Lithos 118:365–382.
Blasi A (1971) Genesi dei noduli a sillimanite nelle anatessiti del Mt. Pélago (Alpi Marittime) in rapporto ai fenomeni di metamorfismo, piegamento e granitizzazione. Mem Soc Geol It 10:167–190.
Blasi A, Schiavinato G (1968) Significato petrologico dei noduli a sillimanite e dei noduli a cordierite diffusi nelle anatessiti biotitiche del M. Pelago (massiccio cristallino dell'Argentera). Boll Soc Geol It 87:253–275.
Bogdanoff S, Ménot RP, Vivier G (1991) Les massifs cristallins externes des alpes occidentales françaises, un fragment de la zone interne varisque. Sci Géol Bull :237–283.
Bogdanoff S, Ploquin A (1980) Les gneiss et migmatites du massif de l'Argentera (Alpes maritimes); apport de deux coupes geochimiques. Bull Soc géol Fr 7:353–358.
Bogdanoff S, Michard A, Mansour M, Poupeau G (2000) Apatite fission track analysis in the Argentera massif: evidence of contrasting denudation rates in the External Crystalline Massifs of the Western Alps. Terra Nova 12:117–125.
Boland JN, Van Roermund HLM (1983) Mechanisms of exsolution in omphacites from high temperature, type B, eclogites. Physics and Chemistry of Minerals, 9:30–37.
Bortolami G, Sacchi R (1968) Osservazioni geologico-petrografiche sui medi valloni di S.Anna e Rio Freddo (Massiccio Cristallino dell'Argentera). Mem Soc Geol It 7:37–64.
Boucarut M (1967) Structure du granite de l'Argentera et style tectonique de l'ensemble de ce massif. C R Acad Sci Paris 264:1573–1576.
Briand B, Bouchardon JL, Capiez, P, Piboule, M (2002) Felsic (A-Type)-Basic (Plume-Induced) Early Palaeozoic bimodal magmatism in the Maures massif (southeastern France). Geol Mag 139:291–311.
Carmignani L, Carosi R, Di Pisa A, Gattiglio M, Musumeci G, Oggiano G, Pertusati PC (1994) The Hercynianchain in Sardinia (Italy). Geodin Acta 7:31–47.
Carosi R, Oggiano G (2002) Transpressional deformation in NW Sardinia (Italy): insights on the tectonic evolution of the Variscan belt. C R Geosci 334:273–278.
Carosi R, Di Pisa A, Iacopini D, Montomoli C, Oggiano G (2004) The structural evolution of the Asinara Island (NW Sardinia, Italy). Geodin Acta 17:309–329.
Carosi R, Frassi C, Montomoli C (2009) Deformation during exhumation of medium-and high-grade metamorphic rocks in the Variscan chain in northern Sardinia (Italy). Geol J 44:280–305.
Carosi R, D'Addario E, Mammoliti E, Montomoli C, Simonetti M (2016) Geology of the northwestern portion of the Ferriere-Mollieres Shear Zone, Argentera Massif, Italy. J Maps 12sup1:466–475.
Carswell DA, Wilson RN, Zhai M (2000) Metamorphic evolution, mineral chemistry and thermobaromety of schists and orthogneisses hosting ultra-high pressure eclogites in the Dabieshan of central China. Lithos 52:121–155.
Cloos M (1993) Lithospheric buoyancy and collisional orogenesis: subduction of oceanic plateaus, continental margins, island arcs, spreading ridges, and seamounts. Geol Soc Am Bull 105:715–737.
Cocks LRM, Torsvik TH (2011) The Palaeozoic geography of Laurentia and western Laurussia: a stable craton with mobile margins. Earth Sci Rev 106:1–51.
Coggon R, Holland JB (2002) Mixing properties of phengitic micas and revised garnetphengite thermobarometers. J Metamorph Geol 20:683–696.
Coleman RG, Lee DE, Beatty LB, Brannock WW (1965) Eclogites and eclogites — their differences and similarities. Geol Soc Am Bull 76:483–508.
Colombo F, Compagnoni R, Lombardo B (1994) Le rocce eclogitiche dei Laghi del Frisson (Argentera sud-orientale, Alpi Marittime). Atti Tic Sci Terra serie speciale 1:75–82.
Compagnoni R, Ferrando S, Lombardo B, Radulesco N, Rubatto D. (2010) Paleo-European crust of the Italian Western Alps: Geological history of the Argentera Massif and comparison with Mont Blanc-Aiguilles Rouges and Maures-Tanneron Massifs. J Virt Explorer 36:3.
Corsin P, Faure-Muret, A (1946) Découverte d'une florule stéphanienne au cirque de Férisson près de Saint-Martin Vésubie (Alpes Maritimes). C R Somm Soc géol Fr :256–257.
Corsin P, Faure-Muret A (1951) Nouvelle flore du Stéphanien à l'est de Saint-Martin Vésubie (Alpes Maritimes), C R Somm Soc géol Fr :57–58.
Corsini M, Ruffet G, Caby R (2004) Alpine and late-hercynian geochronological constrains in the Argentera Massif (Western Alps). Eclogae Geol Helv 97:3–15.

545 Corsini M, Rolland Y (2009) Late evolution of the southern European Variscan belt: exhumation of the lower
546 crust in a context of oblique convergence. C R Geosciences 341:214–223.
547 Corsini M, Bosse V, Féraud G, Demoux A, Crevola G (2010) Exhumation processes during post-collisional
548 stage in the Variscan belt revealed by detailed 40Ar/39Ar study (Tanneron massif, SE France). Int J Earth
549 Sci 96:1–9.
550 Cruciani G, Franceschelli M, Groppo C (2011) P–T evolution of eclogite-facies metabasite from NE Sardinia,
551 Italy: insights into the prograde evolution of Variscan eclogites. Lithos 121:135–150.
552 Cruciani G, Franceschelli M, Groppo C, Oggiano G, Spano ME (2015) Re-equilibration history and P–T path of
553 eclogites from Variscan Sardinia, Italy: A case study from the medium-grade metamorphic complex. Int J
554 Earth Sci 104:797–814.
555 Cruciani G, Franceschelli M, Langone A, Puxedd, M, Scodina M (2017) Nature and age of pre-Variscan eclogite
556 protoliths from the Low- to Medium-Grade Metamorphic Complex of north–central Sardinia (Italy) and
557 comparisons with coeval Sardinian eclogites in the northern Gondwana context. J Geol Soc 172:792–807.
558 Dale J, Holland TJB (2003) Geothermobarometry, P-T paths and metamorphic field gradients of high-pressure
559 rocks from the Adula Nappe, Central Alps. J Metamorph Geol 21(8): 813–829.
560 Debon F, Lemmet M (1999) Evolution of Mg/Fe ratios in late Variscan plutonic rocks from the external
561 crystalline massifs of the Alps (France, Italy, Switzerland). J Petrol 40(7):1151–1185.
562 De Capitani C, Petrakakis K (2010) The computation of equilibrium assemblage diagrams with Theriak/Domino
563 software. Amer Min 95 :1006–1016.
564 Demoux A, Schärer U, Corsini M (2008) Variscan evolution of the Tanneron massif, SE-France, examined
565 through U–Pb monazite ages. J Geol Soc 165:467–478.
566 Diener JFA, Powell R, White RW, Holland TJB (2007) A new thermodynamic model for clino- and
567 orthoamphiboles in the system Na2O–CaO–FeO–MgO–Al2O3–SiO2–H2O–O. J Metamorph Geol 25:631–
568 656.
569 Di Paola S. (2001) Eredità litostratigrafica, strutturale e metamorfica paleozoica nel margine interno Europeo
570 (Grandes Rousses e Argentera), ristrutturato durante l'orogenesi Alpina. Ph.D. Thesis, Università degli
571 Studi di Milano and Université Claude Bernard Lyon.
572 Di Vincenzo G, Carosi R, Palmeri R (2004) The relationship between tectono-metamorphic evolution and argon
573 isotope records in white mica: constraints from in situ 40Ar-39Ar laser analysis of the Variscan Basement
574 of Sardinia. J Petrol 45:1013–1043.
575 Domeier M, Torsvik TH (2014) Plate tectonics in the Late Paleozoic. Geosci Front 5:303–350.
576 Donnelly K E, Goldstein S L, Langmuir C H, Spiegelman M (2004) Origin of enriched ocean ridge basalts and
577 implications for mantle dynamics. Earth Plan Sci Lett 226:347–366.
578 Droop GTR (1983) Pre-Alpine eclogites in the Pennine Basement Complex of the Eastern Alps. J Metamorph
579 Geol 1(1):3–12.
580 Edel JB, Casini L, Oggiano G, Rossi P, Schulmann K (2014) Early Permian 90° clockwise rotation of the
581 Maures–Estérel–Corsica–Sardinia block confirmed by new palaeomagnetic data and followed by a Triassic
582 60° clockwise rotation. In: Schulmann K, Martínez Catalán JR, Lardeaux JM, Janoušek V, Oggiano G
583 (Eds) The Variscan Orogeny: Extent, Timescale and the Formation of the European Crust. Geol Soc
584 London Sp Pub 405:333–361.
585 Edel JB, Schulmann K, Lexa O, Lardeaux J M (2018) Late Palaeozoic palaeomagnetic and tectonic constraints
586 for amalgamation of Pangea supercontinent in the European Variscan belt. Earth Sci Rev 177:589–612.
587 Elter F M, Musumeci G, Pertusati, PC (1990) Late Hercynian shear zones in Sardinia. Tectonophysics,176:387–
588 404.
589 Ernst W G (1971) Metamorphic zonations on presumably subducted lithospheric plates from Japan, California,
590 and the Alps. Contrib Mineral Petrol 34:43–59.
591 Ernst WG, Liou JG (2008) High- and ultrahigh-pressure metamorphism: Past results and future prospects. Am
592 Mineral 93:1771–1786.
593 Ernst WG, Liu J (1998). Experimental phase-equilibrium study of Al-and Ti-contents of calcic amphibole in
594 MORB—A semiquantitative thermobarometer. Am Mineral 83:952–969.
595 Faryad SW, Melcher F, Hoinkes G, Puhl J, Meisel T, Frank W (2002) Relics of eclogite facies metamorphism in
596 the Austroalpine basement, Hochgroessen (Speik complex), Austria. Mineral Petrol 74: 49–73.
597 Faure M, Bé Mézème E, Duguet M, Cartier C, Talbot JY (2005) Paleozoic tectonic evolution of medio-Europa

598 from the example of the French Massif Central and Massif Armoricain. J Virtual Expl 19(5):1–26.
599 Faure M, Lardeaux J M, Ledru P (2009) A review of the pre-Permian geology of the Variscan French Massif
600 Central. C R Geosciences 341:202–213.
601 Faure M, Rossi P, Gaché J, Melleton J, Frei D, Li X, Lin W (2014) Variscan orogeny in Corsica: new structural
602 and geochronological insights, and its place in the Variscan geodynamic framework. Int J Earth Sci
603 103:1533–1551.
604 Faure-Muret A., Fallot P (1955) Carte géologique de la France au 1/50000. Notice de la feuille de St Etienne de
605 Tinée. XXXVI-40. BRGM.
606 Faure-Muret A (1955) Etudes géologiques sur le Massif de l'Argentera-Mercantour et sur ses enveloppes
607 sédimentaires. Paris, Mém Carte Géol France, pp. 336.
608 Ferrando S, Lombardo B, Compagnoni R (2008) Metamorphic history of HP mafic granulites from the Gesso-
609 Stura Terrain (Argentera Massif, Western Alps, Italy). Eur J Mineral 20:777–790.
610 Ferrara G, Malaroda R (1969) Radiometric age of granitic rocks from the Argentera Massif (Maritime Alps).
611 Boll Soc Geol It 88:311–320.
612 Filippi M, Zanoni D, Gosso G, Lardeaux JM, Verati C, Spalla MI (2019) Structure of lamprophyres: a
613 discriminant marker for Variscan and Alpine tectonics in the Argentera-Mercantour Massif, Maritime Alps.
614 Bull Soc géol Fr - Earth Sciences Bulletin 190:12.
615 Franceschelli M, Puxeddu M, Cruciani G, Utzeri D (2007) Metabasites with eclogite facies relics from
616 Variscides in Sardinia, Italy: a review. Int J Earth Sci 96:795–815.
617 Franke W (1989) Variscan plate tectonics in Central Europe – current ideas and open questions. Tectonophysics
618 169:221–228.
619 Franke W (2000) The mid-European segment of the Variscides: tectono-stratigraphic units, terrane boundaries
620 and plate tectonic evolution. Geol Soc Sp Pub London 179:35–61.
621 Franke W, Cocks LRM, Torsvik TH (2017) The Palaeozoic Variscan oceans revisited. Gondwana Res 48:257–
622 284.
623 Fréville K, Trap P, Faure M, Melleton J, Li XH, Lin W, Blein O, Bruguiere O, Poujol M (2018) Structural,
624 metamorphic and geochronological insights on the Variscan evolution of the Alpine basement in the
625 Belledonne Massif (France). Tectonophysics 726:14–42.
626 Gasparik T, Lindsley DH (1980) Phase equilibria at high pressure of pyroxenes containing monovalent and
627 trivalent ions. In: Prewitt CT (Ed) Pyroxenes. Reviews in mineralogy 7. Mineral Soc Amer: 309–339.
628 Gerbault M, Schneider J, Reverso-Peila A, Corsini M (2018) Crustal exhumation during ongoing compression in
629 the Variscan Maures-Tanneron Massif, France-Geological and thermo-mechanical aspects. Tectonophysics
630 746 :439–458.
631 Gerya TV, Perchuk LL, Burg JP (2008) Transient hot channels: Perpetrating and regurgitating ultrahigh-
632 pressure, high-temperature crust–mantle associations in collision belts. Lithos 103:236–256.
633 Giacomini F, Bomparola RM, Ghezzo C (2005) Petrology and geochronology of metabasites with eclogite facies
634 relics from NE Sardinia: constraints for the Palaeozoic evolution of Southern Europe. Lithos 82:221–248.
635 Giacomini F, Braga R, Tiepolo M, Tribuzio R (2007) New constraints on the origin and age of Variscan
636 eclogitic rocks (Ligurian Alps, Italy). Contrib Mineral Petrol 153(1): 29–53.
637 Giacomini F, Dallai L, Carminati E, Tiepolo M, Ghezzo C (2008) Exhumation of a Variscan orogenic complex:
638 insights from the composite granulitic-amphibolitic metamorphic basement of South-East Corsica (France).
639 J Metamorph Geol 26: 403–436.
640 Gosso G, Lardeaux JM, Zanoni D, Volante S, Corsini M, Bersezio R, Mascle J, Spaggiari L, Spalla MI, Zucali
641 M, Giannerini G, Camera L. (2019) Mapping the progressive geologic history at the junction of the Alpine
642 mountain belt and the western Mediterranean ocean. Ofioliti 44:97–110.
643 Graham CM, Powell R (1984) A garnet–hornblende geo-thermometer: calibration testing and application to the
644 Pelona schist, southern California. J Metamorph Geol 2 :13–31.
645 Green E C, Holland TJB, Powell R (2007) An order– disorder model for omphacitic pyroxenes in the system
646 jadeite– diopside hedenbergite–acmite, with applications to eclogitic rocks. Amer Min 92:1181–1189.
647 Guillot S, Di Paola S, Ménot RP, Ledru P, Spalla MI, Gosso G, Schwartz S (2009) Suture zones and importance
648 of strike-slip faulting for Variscan geodynamic reconstructions of the External Crystalline Massifs of the
649 western Alps. Bull Soc géol Fr 6: 483–500.
650 Guillot S, Ménot RP (2009) Paleozoic evolution of the external crystalline massifs of the Western Alps. C R

651 Géoscience 341:253–265.
652 Guiraud M, Powell R, Rebay G (2001) H2O in metamorphism and unexpected behaviour in the preservation of
653 metamorphic assemblages. J Metamorph Geol 19:445–454.
654 Hawthorne FC, Oberti R, Harlow GE, Maresch WV, Martin RF, Schumacher JC, Welch MD (2012)
655 Nomenclature of the amphibole supergroup. Amer Min 97:2031–2048.
656 Herzberg C, Riccio L, Chiesa A, Fornoni A, Gatto GO, Gregnanin A, Piccirillo EM, Scolari, A., 1977.
657 Petrogenetic evolution of a spinelgarnet-lherzolite in the austridic crystalline basement from Val Clapa
658 (Alto Adige, northeastern Italy). Memorie degli Istituti di Geologia e Mineralogia dell'Università di Padova
659 XXX :6–23.
660 Hofmann AW (2003) Sampling mantle heterogeneity through oceanic basalts isotopes and trace elements. In:
661 Carlson RW (Ed) The Mantle and Core. Treatise on Geochemistry 2. Elsevier, New York, pp 61–101.
662 Hofmann AW, Jochum KP, Seufert, M White WM (1986) Nb and Pb in oceanic basalts: new constrains on
663 mantle evolution. Earth Planet Sci Lett 80:299–313.
664 Holland TJB (1990) Activities of components in omphacite solid solutions. Contrib Mineral Petrol 105:446–453.
665 Holland TJB, Powell R (1998) An internally consistent thermodynamic dataset for phases of petrological
666 interest. J Metamorph Geol 16:309–343.
667 Holland TJB, Powell R (2003) Activity-composition relations for phases in petrological calculations: an
668 asymmetric multicomponent formulation. Contrib Mineral Petrol 145:492–501.
669 Innocent C, Michard A, Guerrot C, Hamelin B (2003) U-Pb zircon age of 548 Ma for the leptynites (high-grade
670 felsic rocks) of the central part of the Maures Massif. Geodynamic significance of the so-called leptyno-
671 amphibolitic complexes of the Variscan belt of western Europe. Bull Soc géol Fr 174:585–594.
672 Irvine TNJ Baragar WRA (1971) A guide to the chemical classification of the common volcanic rocks. Can J
673 Earth Sci 8:523–548.
674 Joanny V, Lardeaux JM, Trolliard G, Boudeulle M (1989) La transition omphacite => diopside + plagioclase
675 dans les éclogites du Rouergue (Massif central français): un exemple de précipitation discontinue. C R
676 Acad Sci Paris 309:1929–1930.
677 Joanny V, van Roermund H, Lardeaux JM (1991) The clinopyroxene/plagioclase symplectite in retrograde
678 eclogites: a potential geothermometer. Geol Rundsch 80:303–320.
679 Klinkhammer GP, Elderfield H, Edmond JM, Mitra A (1994) Geochemical implications of rare earth element
680 patterns in hydrothermal fluids from mid-ocean ridges. Geochim Cosmochim Acta 58: 5105–5113.
681 Konzett J, Krenn K, Hauzenberge, C, Whitehouse M, Hoinkes G (2012) High pressure tourmaline formation and
682 fluid activity in Fe–Ti-rich eclogites from the Kreuzeck Mountains, Eastern Alps, Austria. J Petrol 53 :99–
683 125.
684 Krogh-Ravna, E (2000) The garnet-clinopyroxene Fe^{2+}-Mg geothermometer: an updated calibration. J
685 Metamorph Geol 18:211–219.
686 Labanieh S, Chauvel C, Germa A, Quidelleur X (2012) Martinique: a clear case for sediment melting and slab
687 dehydration as a function of distance to the trench. J Petrol 53 :2441–2464.
688 Lardeaux JM (2014a) Deciphering orogeny: a metamorphic perspective. Examples from European Alpine and
689 Variscan belts. Part I: Alpine metamorphism in the western Alps. A review. Bull Soc géol Fr 185:93–114.
690 Lardeaux JM (2014b) Deciphering orogeny: a metamorphic perspective. Examples from European Alpine and
691 Variscan belts. Part II: Variscan metamorphism in the French Massif Central – A review. Bull Soc géol Fr
692 185:281–310.
693 Lardeaux JM, Schulmann K, Faure M, Janoušek V, Lexa O, Skrzypek E, Edel JB, Štípská P (2014) The
694 Moldanubian Zone in the French Massif Central, Vosges/ Schwarzwald and Bohemian Massif revisited:
695 differences and similarities. In: Schulmann K, Martínez Catalán JR, Lardeaux JM, Janoušek V, Oggiano G
696 (Eds) The Variscan Orogeny: Extent, Timescale and the Formation of the European Crust. Geol Soc
697 Londond Spec Publ 405:7–44.
698 Lardeaux JM, Ménot RP, Orsini JB, Rossi P, Naud G, Libourel G (1994) Corsica and Sardinia in the Variscan
699 chain. In: Keppie JD (Ed) Pre- Mesozoic Geology in France and Related Areas. Springer, Berlin, pp 467–
700 479.
701 Lardeaux JM, Ledru P, Daniel I, Duchêne S (2001) The Variscan French Massif Central—a new addition to the
702 ultra-high pressure metamorphic 'club': exhumation processes and geodynamic consequences.
703 Tectonophysics 332:143–167.

Latouche L, Bogdanoff S (1987) Evolution précoce du massif de l'Argentera: apport des eclogites et des granulites. Géol Alp 63:151–164.

Leake BE, Woolley AR, Birch WD, Burke EAJ, Ferraris G, Grice JD, Hawthorne FC, Kisch HJ, Krivovichev VG, Schumacher JC, Stephenson NCN, Whittaker EJW (2004) Nomenclature of amphiboles: additions and revisions to the International Mineralogical Association's amphibole nomenclature. Eur J Mineral 16:191–196.

Ledru P, Lardeaux JM, Santallier D, Autran A, Quenardel JM, Floc'h JP, Lerouge G, Maillet N, Marchand J, Ploquin A (1989) Où sont les nappes dans le Massif central français? Bull Soc géol Fr 8:605–618.

Ledru, P, Courrioux G, Dallain C, Lardeaux JM, Montel JM, Vanderhaeghe O, Vitel G (2001) The Velay dome (French Massif Central): melt generation and granite emplacement during orogenic evolution. Tectonophysics 342:207–237.

Le Fort P (1973) Geologie du Haut-Dauphine cristallin (Alpes Francaises): Etudes pétrologique et structurale de la partie occidentale. Ph.D. thesis, Université Nancy.

Li XH, Faure M, Lin W (2014) From crustal anatexis to mantle melting in the Variscan orogen of Corsica (France): SIMS U–Pb zircon age constraints. Tectonophysics 634:19–30.

Liati A, Gebauer D, Fanning M (2009) Geochronological evolution of HP metamorphic rocks of the Adula nappe, Central Alps, in pre-Alpine and Alpine subduction cycles. J Geol Soc 166: 797–810.

Liégeois JP, Duchesne JC (1981) The Lac Cornu retrograded eclogites (Aiguilles Rouges massif, Western Alps, France): evidence of crustal origin and metasomatic alteration. Lithos 14(1): 35–48.

Lotout C, Pitra P, Poujol M, Anczkiewicz R, Van Den Driessche J (2018) Timing and duration of variscan high-pressure metamorphism in the French Massif Central: A multimethod geochronological study from the Najac Massif. Lithos 308–309:381–394.

Maino M, Dallagiovanna G, Gaggero L, Seno S, Tiepolo M (2012) U-Pb zircon geochronological and petrographic constraints on late to post-collisional Variscan magmatism and metamorphism in the Ligurian Alps, Italy. Geol J 47(6):632–652.

Malaroda R, Carraro F, Dal Piaz GV, Franceschetti B, Sturani C, Zanella E (1970) Carta geologica del Massiccio dell'Argentera alla scala 1:50.000 e note illustrative. Mem Soc Geol It 9:557–663.

Malaroda R, Schiavinato G (1958) Le anatessiti dell'Argentera. Rend Soc Min It 14:249–274.

Malaroda R, Schiavinato G (1960). Agmatiti e migmatiti anfiboliche omogenee nel settore meridionale del Massiccio dell'Argentera. Rend Soc Min It 16:335–346.

Martínez Catalán, JR, Arenas R, García FD, Cuadra PG, Gómez-Barreiro, J, Abati J, Castiñeiras P, Fernández-Suárez J, Martínez SS, Andonaegui P, (2007) Space and time in the tectonic evolution of the northwestern Iberian Massif: implications for the Variscan belt. Geol Soc Am Mem 200:403–423.

Martínez Catalán JR, Arena, R, Abat, J, SánchezMartínez S, Díaz García, F, Fernández- Suárez J, González Cuadra P, Castiñeiras P, Gómez Barreiro J, Díez Montes A, González Clavijo E, Rubio Pascual FJ, Andonaegui P, Jeffries TE, Alcock JE, Díez Fernández R, López Carmona A (2009) A rootless suture and the loss of the roots of a mountain chain: the Variscan belt of NW Iberia. C R Geosciences 341:114–126.

Matte P (1986) Tectonics and plate tectonics model for the Variscan belt of Europe. Tectonophysics 126:329–374.

Matte P (2001) The Variscan collage and orogeny (480–290 Ma) and the tectonic definition of the Armorica microplate: a review. Terra Nova 13:122–128.

Matte P, Burg JP (1981) Sutures, thrusts and nappes in the Variscan arc of western Europe. Plate tectonics interpretation. Geol Soc London Sp Pub 8:353–358.

Matte P, Maluski H, Rajlich P, Franke W (1990) Terrane boundaries in the Bohemian Massif: result of large-scale Variscan shearing. Tectonophysics 177:151–170.

McKenzie D, O'Nions RK (1991) Partial melt distributions from inversion of rare earth element concentrations. J Petrol 32:1021–1091.

McKerrow WS, Mac Niocaill C, Ahlberg P, Clayton G, Cleal CJ, Eagar RMC (2000) The Late Palaeozoic relations between Gondwana and Laurussia. Geol Soc Lond Spec Publ 179:9–20.

Medaris L G, Jelinek E, Misar Z (1995) Czech eclogites: terrane settings and implications for Variscan tectonic evolution of the Bohemian Massif. Euro J Mineral 7:7–28.

Melcher F, Meisel T, Puhl J, Koller F (2002) Petrogenesis and geotectonic setting of ultramafic rocks in the Eastern Alps: constraints from geochemistry. Lithos 65(1–2):69–112.

Meschede M (1986) A method of discriminating between different types of mid-ocean ridge basalts and continental tholeiites with the Nb-Zr-Y diagram. Chem Geol 56:207–218.
Messiga B, Tribuzio R, Caucia F (1992) Amphibole evolution in Variscan eclogite-amphibolites from the Savona crystalline massif (Western Ligurian Alps, Italy): controls on the decompressional P-T-t path. Lithos 27: 215–230.
Michard A, Albarède F (1986) The REE content of some hydrothermal fluids. Chem Geol 55:51–60.
Miyashiro A (1961) Evolution of Metamorphic Belts. J Petrol. 2:277–311.
Morimoto N (1988). Nomenclature of pyroxenes. Mineral Petrol 39:55–76.
Morten L, Nimis P, Rampone E (2004) Records of mantle–crust exchange processes during continental subduction–exhumation in the Nonsberg-Ultental garnet peridotites (eastern Alps). A review. Periodico di Mineralogia 73:119–129.
Musumeci G, Colombo F (2002) Late Visean mylonitic granitoids in the Argentera Massif (Western Alps, Italy): age and kinematic constraints on the Ferriere-Mollières shear zone. C. R. Geosciences 334:213–220.
Nussbaum C, Marquer D, Biino GG (1998) Two subduction events in a polycyclic basement: Alpine and pre-Alpine high-pressure metamorphism in the Suretta nappe, Swiss Eastern Alps. J Metamorph Geol 16:591–605.
Oliot E, Melleton J, Schneider J, Corsini M, Gardien, V, Rolland Y (2015) Variscan crustal thickening in the Maures-Tanneron massif (South Variscan belt, France): new in situ monazite U-Th-Pb chemical dating of high-grade rocks. Bull Soc géol Fr 186:145–169
Otten MT (1984) Metamorphism and deformation during and after cooling of the Artfjallet gabbro. J Geol Soc 141:189–190.
Palagi P, Laporte D, Lardeaux J M, Menot R P, Orsini JB (1985) Identification d'un complexe leptyno-amphibolique au sein des "gneiss de Belgodère" (Corse occidentale). C R Acad Sci Paris 301:1047–1052.
Palmeri R, Fanning M, Franceschelli M, Memmi I, Ricci CA (2004) SHRIMP dating of zircons in eclogite from the Variscan basement in north-eastern Sardinia (Italy). Neu Jahr für Min Monat 6:275–288.
Pattison DRM (1991) Infiltration-driven anatexis in granulite facies metagabbro, Grenville Province, Ontario, Canada. J Metamorph Geol 9: 315–332.
Pearce JA (1996) A user's guide to basalt discrimination diagrams. In: Wyman DA (Ed) Trace Element Geochemistry of Volcanic Rocks: Applications for Massive Sulphide Exploration. Geol Ass Canada, Short Course Notes 12:79–113.
Pearce JA (2008) Geochemical fingerprinting of oceanic basalts with applications to ophiolite classification and the search for Archean oceanic crust. Lithos 100:14–48.
Polino R, Dal Piaz GV, Gosso G (1990) Tectonic erosion at the Adria margin and accretionary processes for the Cretaceous orogeny of the Alps. Mem Soc géol Fr 156:345–367.
Rebay G, Powell R, Diener J (2010) Calculated phase equilibria for a MORB composition in a P T window, 450–650°C and 18–28 kbar: the stability of eclogite. J Metamorph Geol 28:635–645.
Regorda A, Lardeaux JM, Roda M, Marotta AM, Spalla MI (2019) How many subductions in the Variscan orogeny? Insights from numerical models. Geosci Front. DOI: 10.1016/j.gsf.2019.10.005
Roda M, Regorda A, Spalla MI, Marotta AM (2019) What drives Alpine Tethys opening? Clues from the review of geological data and model predictions. Geol J 54:2646–2664.
Rossi P, Oggiano G, Cocherie A (2009) A restored section of the ''southern Variscan realm'' across the Corsica–Sardinia microcontinent. C R Geosciences 341:224–238.
Rudnick R, Fountain DM (1995) Nature and composition of the continental crust: A lower crustal perspective. Rev Geophysics 33:267–309.
Rubatto D, Schaltegger U, Lombardo B, Colombo F, Compagnoni R (2001) Complex Paleozoic magmatic and metamorphic evolution in the Argentera Massif (Western Alps), resolved with U-Pb dating. Schweiz Mineral Petrogr Mitt 81:213–228.
Rubatto D, Ferrando S, Compagnoni R, Lombardo B (2010) Carboniferous high-pressure metamorphism of Ordovician protoliths in the Argentera Massif (Italy), Southern European Variscan belt. Lithos 116:65–76.
Saccani E (2015) A new method of discriminating different types of post-Archean ophiolitic basalts and their tectonic significance using Th-Nb and Ce-Dy-Yb systematics. Geosc Front 6:481–501.
Sanchez G, Rolland Y, Schreiber D, Giannerini G, Corsini M, Lardeaux JM (2010) The active fault system of SW Alps. J Geodyn 49(5):296–302.

Sanchez G, Rolland Y, Schneider J, Corsini M, Oliot E, Goncalves P, Verati C, Lardeaux JM, Marquer D (2011) Dating low-temperature deformation by 40Ar/39Ar on white mica, insights from the Argentera-Mercantour Massif (SW Alps). Lithos 125:521–536.

Schmidt MW, Poli S (1998) Experimentally based water budgets for dehydrating slabs and consequences for arc magma generation. Earth Planet Sci Lett 163:361–379.

Schmid SM, Fügenschuh B, Kissling E, Schuster R (2004) Tectonic map and overall architecture of the Alpine orogen. Eclog Geol Helv 97:93–117.

Schreiber D, Lardeaux JM, Martelet G, Courrioux G, Guillen A (2010) 3-D modelling of Alpine Mohos in Southwestern Alps. Geophys J Int 180:961–975.

Schneider J, Corsini M, Reverso-Peila A, Lardeaux JM (2014) Thermal and mechanical evolution of an orogenic wedge during Variscan collision: an example in the Maures–Tanneron Massif (SE France). In: Schulmann K, Martínez Catalán JR, Lardeaux JM, Janoušek V, Oggiano G (Eds) The Variscan Orogeny: Extent, Timescale and the Formation of the European Crust. Geol Soc London Spec Publ 405:313–331.

Schulmann K, Kröner A, Hegner E, Wend, I, Konopasek J, Lexa O, Stipská P (2005) Chronological constraints on the pre-orogenic history, burial and exhumation of deep-seated rocks along the eastern margin of the Variscan Orogen, Bohemian Massif, Czech Republic. Amer J Sci 305:407–448.

Schulmann K, Konopásek J, Janoušek V, Lexa O, Lardeaux JM, Edel JB, Stípská P, Ulrich S (2009) An Andean type Palaeozoic convergence in the Bohemian Massif. C R Geosciences 341:266–286.

Schulmann K, Lexa O, Janoušek V, Lardeaux JM, Edel JB (2014) Anatomy of a diffuse cryptic suture zone: An example from the Bohemian Massif, European Variscides. Geology 42:275–278.

Schultz B, Bombach K, Pawlig S, Brätz H (2004) Neoproterozoic to Early-Palaeozoic magmatic evolution in the Gondwana-derived Austroalpine basement to the south of the Tauern Window (Eastern Alps). Int J Earth Sci 93:824–843.

Schwartz S, Lardeaux JM, Tricart P, Guillot S, Labrin E (2007) Diachronous exhumation of HP-LT metamorphic rocks from south-western Alps: evidence from fission track analysis. Terra Nova 19:133–140.

Schweinehage R, Massonne H (1999) Geochemistry and metamorphic evolution of metabasites from the Silvretta nappe, Eastern Alps. Memorie Scienze Geologiche 51(1):191– 203.

Shervais JW (1982) Ti-V plots and the petrogenesis of modern and ophiolitic lavas. Earth Planet Sci Lett 59:101–118.

Simonetti M, Carosi R, Montomoli C, Langone A, D'Addario E, Mammoliti E (2018) Kinematic and geochronological constraints on shear deformation in the Ferriere-Mollières shear zone (Argentera-Mercantour Massif, Western Alps): implications for the evolution of the Southern European Variscan Belt. Int J of Earth Sci 107:2163–2189.

Spalla MI, Marotta AM (2007) P-T evolutions vs. numerical modelling: a key to unravel the Paleozoic to early-Mesozoic tectonic evolution of the Alpine area. Per Mineral 76:267–308.

Spalla M I, Zanoni D, Marotta A M, Rebay G, Roda M, Zucali M, Gosso G (2014) The transition from Variscan collision to continental break-up in the Alps: insights from the comparison between natural data and numerical model predictions. In: Schulmann, K, Martínez Catalán JR, Lardeaux JM, Janoušek V, Oggiano G (Eds) The Variscan Orogeny: Extent, Timescale and the Formation of the European Crust. Geol Soc London Spec Pub 405:363–400.

Spear FS (1993) Metamorphic Phase Equilibria and Pressure-Temperature-Time Paths. Min Soc Am Monograph Series 1 pp. 789.

Spiess R, Cesare B, Mazzoli C, Sassi R, Sassi FP (2010) The crystalline basement of the Adria microplate in the eastern Alps: a review of the palaeo- structural evolution from the Neoproterozoic to the Cenozoic. Rend Lincei Sci Fis Nat 21:31–50.

Stampfli GM, Borel, G (2002) A plate tectonic model for the Paleozoic and Mesozoic constrained by dynamic plate boundaries and restored synthetic oceanic isochrons. Earth Planet Sci Lett 196:17-33.

Stampfli GM, Hochard C, Vérard C, Wilhem C, VonRaumer J (2013) The formation of Pangea. Tectonophysics 593:1–19.

Štípská P, Schulmann K, Kröner A (2004) Vertical extrusion and middle crustal spreading of omphacite granulite: a model of syn-convergent exhumation (Bohemian Massif, Czech Republic). J Metamorph Geol 22:179–198.

Štípská P, Powell R (2005) Constraining the P–T path of a MORB-type eclogite using pseudosections, garnet

zoning and garnet-clinopyroxene thermometry: an example from the Bohemian Massif. J Metamorph Geol 23:725–743.

Štípská P, Powell R, Racek M, Lexa O (2014) Intermediate granulite produced by transformation of eclogite at a felsic granulite contact, in Blansky les, Bohemian Massif. J Metamorph Geol 32:347–370.

Sun SS, McDonough WF (1989) Chemical and isotopic systematics of oceanic basalts: implications for mantle composition and processes. In: Saunders AD, Norry MJ (Eds) Magmatism in the Ocean Basins. Geol Soc London Spec Publ 42:313–345.

Tait JA, Bachtadse V, Franke W, Soffel HC (1997) Geodynamic evolution of the European Variscan fold belt: palaeomagnetic and geological constraints. Geol Rundsch 86:585–598.

Tomkins HS, Powell R, Ellis DJ (2007) The pressure dependence of the zirconium-in-rutile thermometer. J Metamorph Geol 25:703–713.

Thompson R., Morrison MA, Dickin A, Hendry GL (1983) Continental flood basalts arachnids rule OK? In: Hawkesworth CJ, Norry MJ (Eds) Continental Basalts and Mantle Xenoliths. Shiva Publications, India, pp 158–185.

Torsvik TH, Smethurst MA, Briden JC, Sturt BA (1990) A review of Paleozoic paleomagnetic data from Europe and their paleogeographic implications. In: Palaeozoic Palaeogeography and Biogeography 12. Geological Soc Publishing House, Bath, pp 25–41.

Torsvik TH, Smethurst M, Meert JG, Van der Voo R, McKerrow W, Brasier M, Sturt B, Walderhaug H (1996) Continental break-up and collision in the Neoproterozoic and Palaeozoic—a tale of Baltica and Laurentia. Earth Sci. Rev. 40:229–258.

Tumiati S, Thöni M, Nimis P, Martin S, Mair V (2003) Mantle-crust interactions during Variscan subduction in the Eastern Alps (Nonsberg-Ulten zone): Geochronology and new petrological constraints. Earth Planet Sci Lett 210(3–4):509–526.

Von Raumer JF (1984) The External Massifs, relics of Variscan basement in the Alps, Geol Rundsch 73:1–31.

Von Raumer JF, Abrecht J, Bussy F, Lombardo B, Ménot RP, Schaltegger U (1999) The Palaeozoic metamorphic evolution of the Alpine External Massifs. Schweiz Mineral Petrogr Mitt 79:5–22.

Von Raumer JF, Stampfli GM, Borel G, Bussy F (2002) Organization of pre-Variscan basement areas at the north- Gondwana margin. Int J Earth Sci 91:35–52.

Von Raumer JF, Stampfli GM, Bussy F (2003) Gondwana-derived microcontinents — the constituents of the Variscan and Alpine collisional orogens. Tectnophysics 365:7–22.

Von Raumer JF, Bussy F, Stampfli GM (2009) The Variscan evolution in the External massifs of the Alps and place in their Variscan framework. C R Geosciences 341:239–252.

Von Raumer JF, Bussy F, Schaltegger U, Schulz B, Stampfli GM (2013) Pre Mesozoic-Alpine basements – their place in the European Paleozoic framework. GSA Bulletin, 125:89–108.

Watson EB, Wark DA, Thomas JB (2006) Crystallization thermometers for zircon and rutile. Contrib Mineral Petrol 151:413–433.

Winchester JA, Floyd PA (1977) Geochemical discrimination of different magma series and their differentiation products using immobile elements. Chem Geol 20:325–343.

White RW, Powell R, Holland TJB, Worley BA (2000) The effect of TiO2 and Fe2O3 on metapelitic assemblages at greenschist and amphibolite facies conditions: mineral equilibria calculations in the system: K2O–FeO–MgO–Al2O3–SiO2–H2O–TiO2–Fe2O3. J Metamorph Geol 18:497–511.

White RW, Powell R, Clarke GL (2002) The interpretation of reaction textures in Fe-rich metapelitic granulites of the Musgrave Block, central Australia: constraints from mineral equilibria calculations in the system K2O–FeO–MgO– Al2O3–SiO2–H2O–TiO2–Fe2O3. J Metamorph Geol 20:41–55.

White RW, Powell R, Holland TJB. (2007) Progress relating to calculation of partial melting equilibria for metapelites. J Metamorph Geol 25:511–527.

Zimmermann VR, Franz G (1989) Die Eklogite der Unteren Schieferhülle; Frosnitztal/Südvenediger (Tauern, Österreich). Mittelungen der Östereichischen Geologischen Gesellschaft 81:167–188.

Figure captions

Fig. 1: The Argentera-Mecantour Massif in the Alpine arc (after Spalla et al., 2014; Regorda et al., 2019). Black stars: Eclogites known in the pre-Alpine basements from different alpine zones; star labels individuate Alpine and Sardinian eclogites as listed in "Online Resource 10". Inset shows the Alpine arc in the framework of the European Variscan belt. Inset labels: Arm - Armorican Massif; BCBF - Bristol Channel-Bray Fault; BM - Bohemian Massif; Ca - Cantabrian terrane; Cib - Central Iberian; Co - Corsica; FMC - French Massif Central; GSBS - Galicia-Southern Brittany Suture; MT - Maures-Tanneron Massif; OM - Ossa Morena; Py - Pyrenees; Sa - Sardinia; Si - Sicilian-Apulian basements; SP - South Portuguese Zone; WL - West Asturian-Leonese.

Fig. 2: Geological map of the Argentera-Mercantour Massif (after Faure-Muret, 1955, Malaroda et al. 1970, Corsini et al., 2004, Carosi et al. 2016 and Gosso et al. 2019). FMSZ - Ferrere-Mollières Shear Zone. CG – Central Granite. 1 Eclogite occurrences and sampling localities with yellow stars; 2 Migmatitic paragneisses; 3 Migmatitic orthogneisses and metavolcanics; 4 Amphibolites; 5 Syn-tectonic diorites; 6 leucocratic cordierite-bearing anatexites; 7 Amphibolite to greenschistfacies mylonites; 8 Granitoids; 9 Carbonaceous schists, conglomerates, and siliciclastic sandstones (late Carboniferous); 10 -Permian to Eocene sequences; 11 late- to post-Alpine faults; 12 Penninic Front; 13 Greenschist-facies mylonites. White contours labelled a and b locate the maps of Fig. 5 and 6, respectively.

Fig. 3: Eclogitic boudins. (a) Col de Fenestre– Pas des Ladres (France) eclogitic boudin in metatexites; (b) Balma Ghiliè valley (Italy) eclogite within paragneisses; (c) Monte Matto (Italy) boudin of eclogite in cordierite bearing diatexites; (d) Lac Niré (France) eclogite within paragneisses; (e) Lac Long eclogitic boudin in metatexites.

Fig. 4: Retrogressed eclogites. (a) Lago Brocan (Italy) coronas of amphibole around garnets; (b) Lac Niré (France) eclogite with plagioclase around garnets.

Fig. 5: Geological map of the high Gordolasque valley at the Italian-French border. (a) Structural map.
(b) Detailed map of eclogite boudin outcropping north of the Lac Long and cross-section.

Fig. 6: Structural map of upper Valasco Valley (Italy). In the inset detailed form-surface map located with a black star in the structural map, close to Lago Inferiore di Valscura.

Fig. 7: Geochemistry of Argentera-Mercantour eclogites in the Al2O3 vs. TiO2 diagram after Konzett et al. 2012 (7a) and in the AFM diagram after Irvine and Baragar, 1971 (7b).

Fig. 8: Chemical compositions of eclogites in the Y-Nb-Zr (8a after Meschede, 1986), the Th/Yb versus Ta/Yb (8b after Pierce, 1982) and in the N-MORB normalized Th-Nb (8c after Saccani, 2015) diagrams. Fields hatched in grey represent available chemical compositions of Sardinian eclogites (see text for discussion and references).

Fig. 9: Primitive mantle normalized REE (a) and LILEs HFSEs (b) patterns of eclogites. N-MORB, E-MORB and OIB compositions after Sun and McDonough (1989).

Fig. 10: Photomicrographs of eclogites. (a) Clinopyroxene-plagioclase symplectite (crossed polars, lac Niré, France). Progressive decrease of lamellae size from center to rim; (b) Evolution of the symplectite, from coarse clinopyroxene lamellaes (with Jadeite content of 42 mol%) to thinner lamellaes (with jadeite content of 15 mol%), crossed polars, Pas des Ladres (France). Gt - Garnet; Pl - Plagioclase; Amp - Amphibole. (c) Re-equilibrated eclogites with diopside-plagioclase symplectites. Relict amphibole 1 green cores are rimmed by brown Ti rich amphibole 2 that together with plagioclase occurs in coronas around garnets (plane polarized light, Lago Brocan, Italy); (d) Detail on the plagioclase-amphibole 2 coronas around garnet; (e) Inclusions of quartz, amphibole 1 and rutile in garnet (BSE image, Brocan Lake, Italy); (f) Diopside-plagioclase symplectite replacing omphacite (BSE image, sample 0878, Valasco Valley, Italy).

Fig. 11: Composition of clinopyroxenes (a), garnets (b), feldspaths (c) and amphiboles (d) from Argentera eclogites. In all the diagrams minerals from Lac Niré, Lac Long and Pas de Ladres eclogites are represented by stars. Italian eclogites are circles. Different colors have been used for minerals from Valasco Valley: in the diagram 11(a) of Morimoto (1988) black and grey circles represent the recalculated compositions of omphacites and clinopyroxene 2 respectively. In comparison, omphacite of Lac Niré appears in black stars. In Na/Na+Ca vs Al/Al+Si diagram 11(d), stars locate the end-member compositions labelled as follows: ACT - Actinolite, BAR - Barroisite, ED - Edenite, GL - Glaucophane; KTP - Katophorite, PRG - Pargasite, SAD - Sadanagaite, TS - Tschermakite, WIN - Winchite.

Fig. 12: P-T pseudosections calculated from Valasco Valley (a, CARA884) and Lac Long (b, LL13). The red line divides the P-T field of plagioclase bearing assemblages, towards higher temperatures, from assemblages without plagioclase, towards higher pressures. The shaded light blue fields represent the P-T conditions determined using classic geothermobarometry for the eclogite-facies assemblage. Univariant lines are thick.
For pseudosection (a), assemblages in the numbered fields are as follow: 1 - garnet, 2 clinopyroxenes, rutile, quartz; 2 - garnet, amphibole, 2 clinopyroxenes, rutile, quartz; 3 - garnet, amphibole, 2 clinopyroxenes, rutile, clinozoisite, quartz; 4 - garnet, 2 amphiboles, 2 clinopyroxenes, rutile, quartz; 5 - garnet, 2 amphiboles, clinopyroxene, clinozoisite, rutile, quartz; 6 - garnet, amphibole, clinopyroxene, titanite, clinozoisite, rutile, quartz; 7 - garnet, amphibole, clinopyroxene, titanite, clinozoisite, quartz; 8 - garnet, amphibole, titanite, clinozoisite, quartz; 9 - garnet, amphibole, clinopyroxene, titanite, quartz; 10 - garnet, amphibole, clinopyroxene, titanite, rutile, quartz. For pseudosection (b), numbered fields match with the following assemblages: 1 - garnet, white mica, 2 amphiboles, clinopyroxene, quartz, rutile; 2 - garnet, white mica, 2 amphiboles, clinopyroxene, quartz, rutile, clinozoisite; 3 - garnet, biotite, white mica, amphibole, 2 clinopyroxenes, quartz, rutile; 4 - garnet, biotite, amphibole, 2 clinopyroxenes, quartz, rutile; 5 - garnet, biotite, white mica, amphibole, clinopyroxene, quartz, rutile; 6 – garnet, biotite, white mica, amphibole, clinopyroxene, quartz, rutile, clinozoisite; 7 - garnet, biotite, amphibole, clinopyroxene, quartz, rutile, titanite; 8 – garnet, biotite, amphibole, quartz, rutile, sphene; 9 - garnet, biotite, amphibole, clinopyroxene, quartz, rutile, clinozoisite; 10 – plaglioclase, garnet, biotite, amphibole, quartz, rutile; 11 - plagioclase, garnet, biotite, amphibole, quartz, rutile, titanite; 12 - garnet, biotite, clinopyroxene, quartz, rutile; 13 – plagioclase, garnet, biotite, clinopyroxene, quartz, rutile. Some very small fields have not been numbered.

Fig. 13: 40Ar/39Ar age spectrum diagram performed in amphibole from Lac Long sample.

Fig. 14: P-T conditions (violet square) of studied eclogites compared with metamorphic gradients (after Miyashiro, 1961; Ernst, 1971; Spear, 1993) and geotherms after Cloos (1993): (1) near spreading ridge or volcanic arc, (2) normal gradient of old plate interior, (3) warm subduction zones, and (4) cold subduction zones. Vo represents the initial unperturbed geotherm. (a) P-T conditions of Argentera eclogites compared with eclogites from Helvetic-Dauphinois zone and Sardinian eclogites. (b) P-T conditions of Argentera eclogites compared with eclogites from Penninic and Austro-Alpines zones. Box labels refer to locations in Figure 1 and descriptions in “Online Resource 10”.

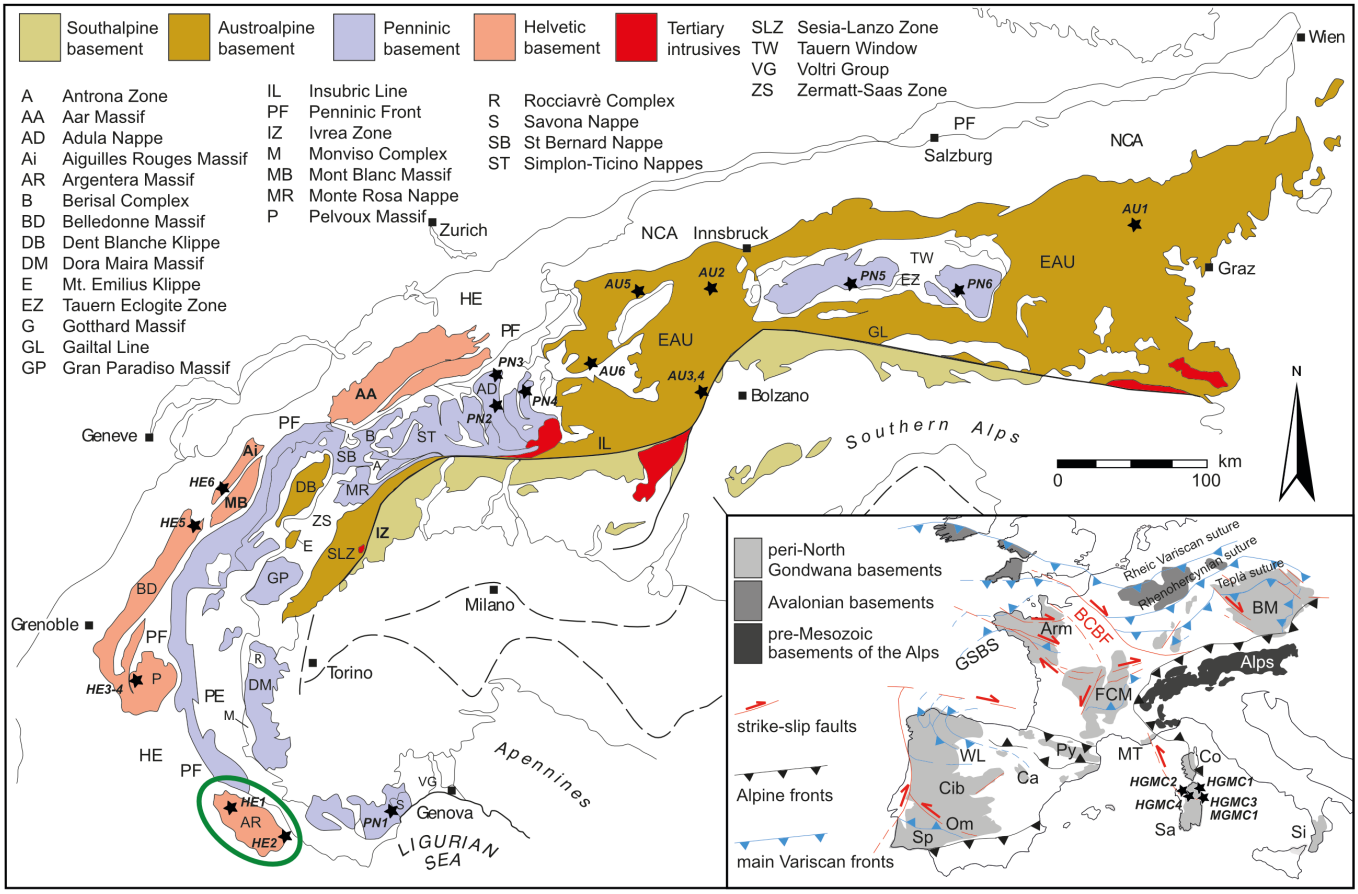
Southalpine basement
Austroalpine basement
Penninic basement
Helvetic basement
Tertiary intrusives
SLZ Sesia-Lanzo Zone
TW Tauern Window
VG Voltri Group
ZS Zermatt-Saas Zone
A Antrona Zone
AA Aar Massif
AD Adula Nappe
Ai Aiguilles Rouges Massif
AR Argentera Massif
B Berisal Complex
BD Belledonne Massif
DB Dent Blanche Klippe
DM Dora Maira Massif
E Mt. Emilius Klippe
EZ Tauern Eclogite Zone
G Gotthard Massif
GL Gailtal Line
GP Gran Paradiso Massif
IL Insubric Line
PF Penninic Front
IZ Ivrea Zone
M Monviso Complex
MB Mont Blanc Massif
MR Monte Rosa Nappe
P Pelvoux Massif
R Rocciavrè Complex
S Savona Nappe
SB St Bernard Nappe
ST Simplon-Ticino Nappes
Wien
Salzburg
NCA
Innsbruck
Zurich
Graz
Bolzano
Geneve
Grenoble
Milano
Torino
Genova
LIGURIAN SEA
Apennines
Southern Alps
HE
PF
AA
EAU
TW
EZ
GL
IL
AD
B
ST
SB
A
DB
MR
ZS
E
SLZ
IZ
GP
BD
Ai
MB
R
DM
M
PE
S
VG
AR
AU1
AU2
AU3,4
AU5
AU6
PN1
PN2
PN3
PN4
PN5
PN6
HE1
HE2
HE3-4
HE5
HE6
P
N
km
0
100
peri-North Gondwana basements
Avalonian basements
pre-Mesozoic basements of the Alps
strike-slip faults
Alpine fronts
main Variscan fronts
Rheic Variscan suture
Rhenohercynian suture
Tépla suture
BCBF
GSBS
Arm
BM
Alps
FCM
MT
Co
Py
WL
Ca
Cib
Om
Sp
Sa
Si
HGMC1
HGMC2
HGMC3
HGMC4
MGMC1

FIGURE 1

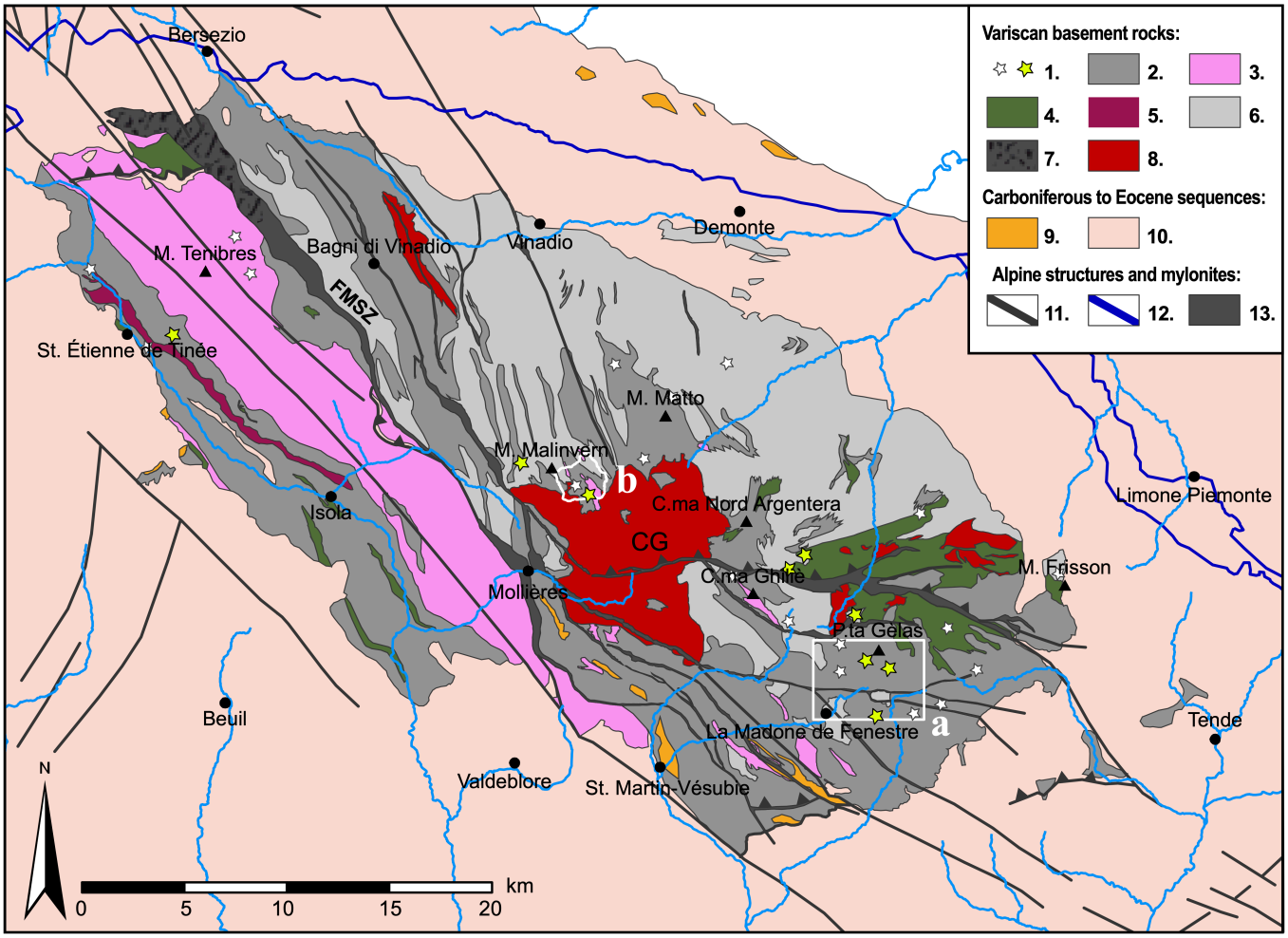
Variscan basement rocks:
1.
2.
3.
4.
5.
6.
7.
8.
Carboniferous to Eocene sequences:
9.
10.
Alpine structures and mylonites:
11.
12.
13.
Bersezio
M. Tenibres
Bagni di Vinadio
Vinadio
Demonte
FMSZ
St. Étienne de Tinée
M. Matto
M. Malinvern
b
Isola
C.ma Nord Argentera
CG
Limone Piemonte
C.ma Ghilie
M. Frisson
Mollières
P.ta Gelas
a
Beuil
La Madone de Fenestre
Tende
Valdeblore
St. Martin-Vésubie
N
0
5
10
15
20
km

FIGURE 2

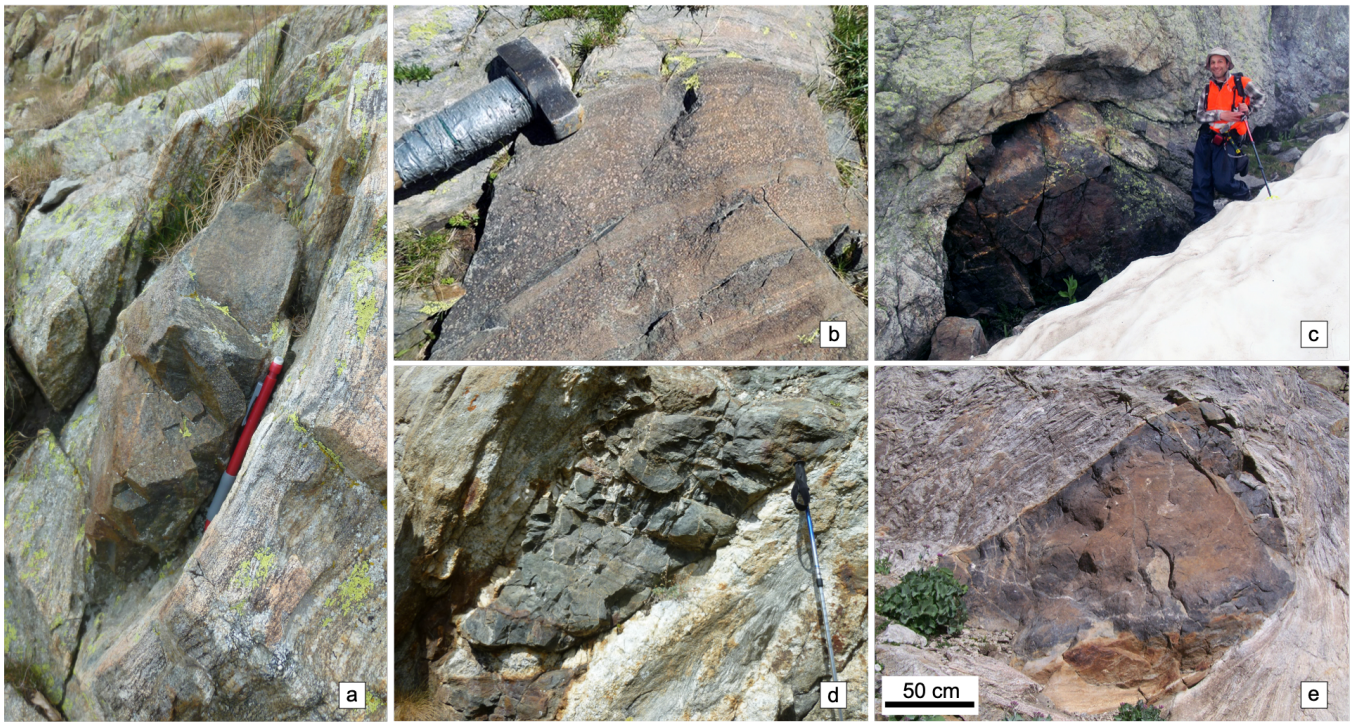

FIGURE 3

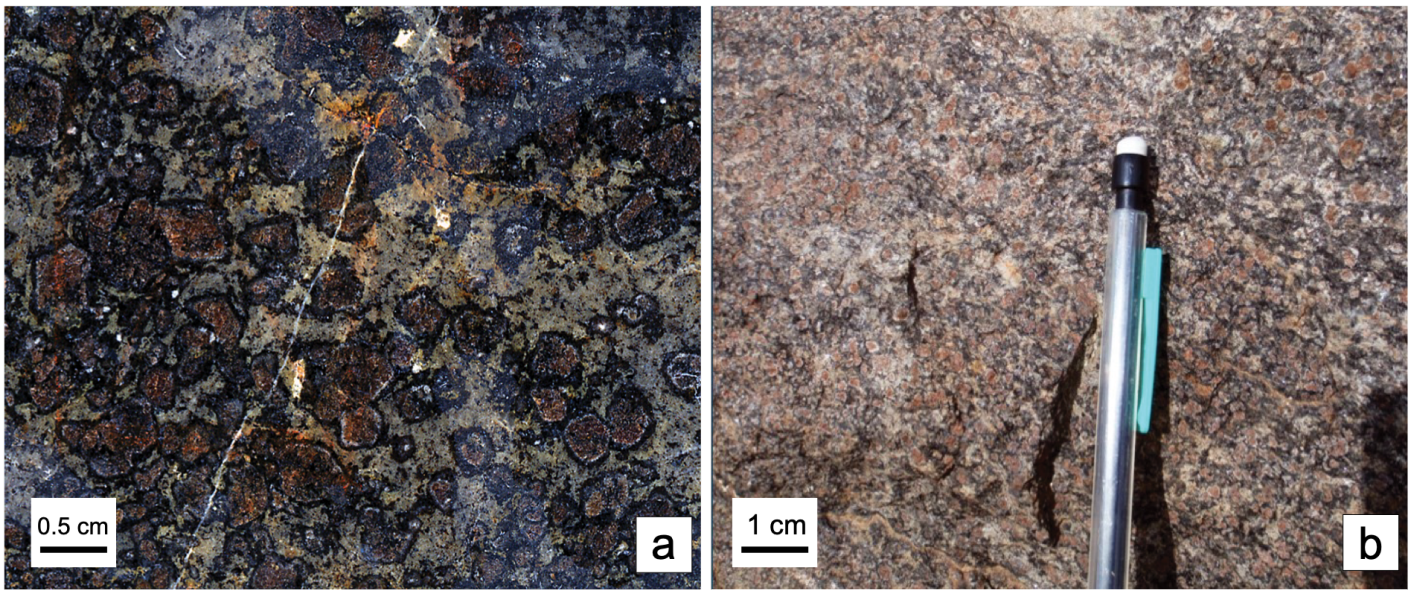

FIGURE 4

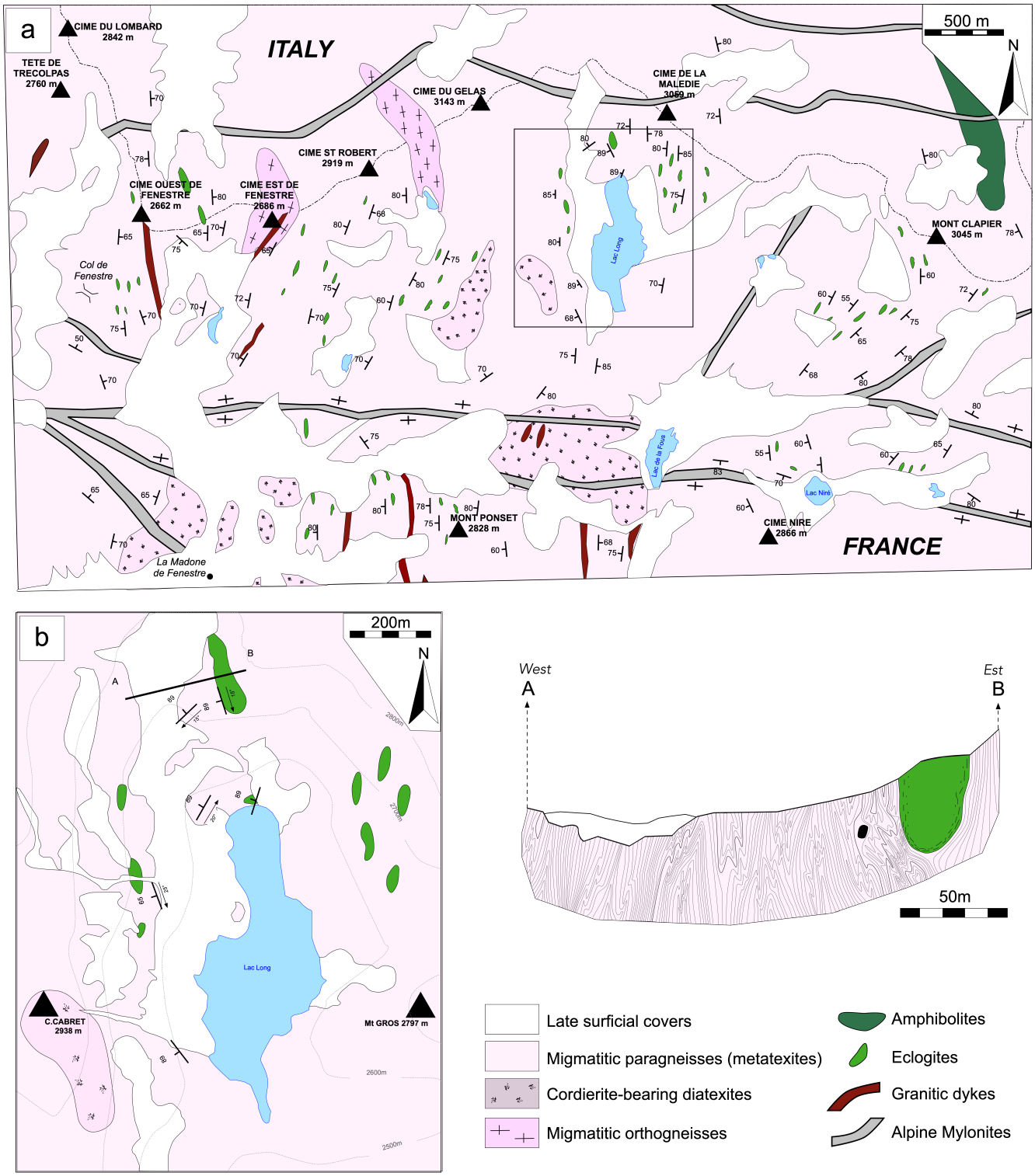
a
CIME DU LOMBARD
2842 m
ITALY
TETE DE
TRECOLPAS
2760 m
CIME DU GELAS
3143 m
CIME DE LA
MALEDIE
3059 m
500 m
N
CIME ST ROBERT
2919 m
CIME OUEST DE
FENESTRE
2662 m
CIME EST DE
FENESTRE
2686 m
Col de
Fenestre
Lac Long
MONT CLAPIER
3045 m
Lac de la Fous
Lac Nire
MONT PONSET
2828 m
CIME NIRE
2866 m
FRANCE
La Madone
de Fenestre
b
200m
N
A
B
Lac Long
C.CABRET
2938 m
Mt GROS 2797 m
2600m
2500m
West
A
Est
B
50m
Late surficial covers
Migmatitic paragneisses (metatexites)
Cordierite-bearing diatexites
Migmatitic orthogneisses
Amphibolites
Eclogites
Granitic dykes
Alpine Mylonites

FIGURE 5

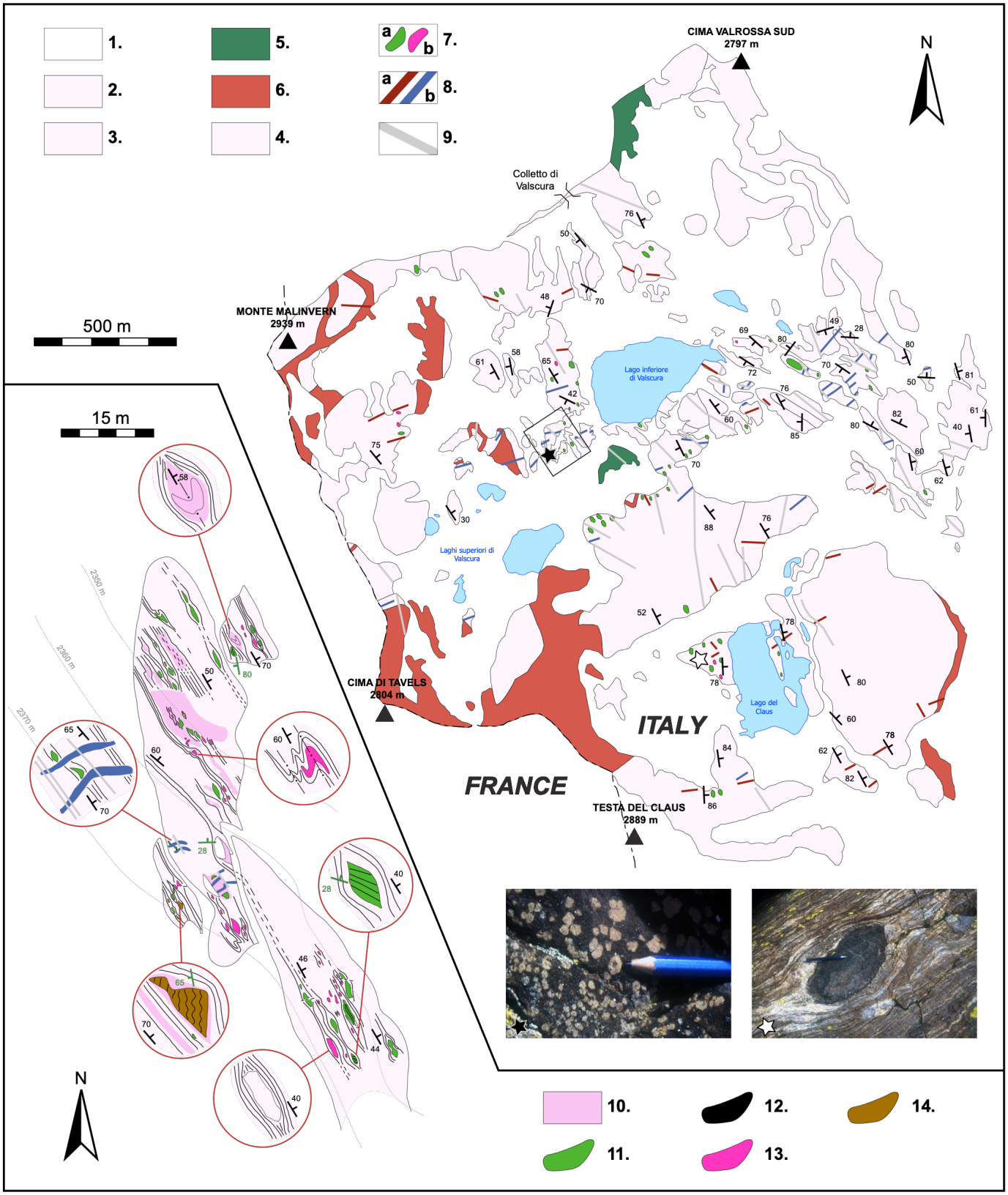
1.
2.
3.
4.
5.
6.
7.
8.
9.
10.
11.
12.
13.
14.
CIMA VALROSSA SUD
2797 m
N
Colletto di
Valscura
MONTE MALINVERN
2939 m
500 m
Lago inferiore
di Valscura
Laghi superiori di
Valscura
CIMA DI TAVELS
2804 m
ITALY
FRANCE
Lago del
Claus
TESTA DEL CLAUS
2889 m
15 m
2390 m
2380 m
2370 m
N

FIGURE 6

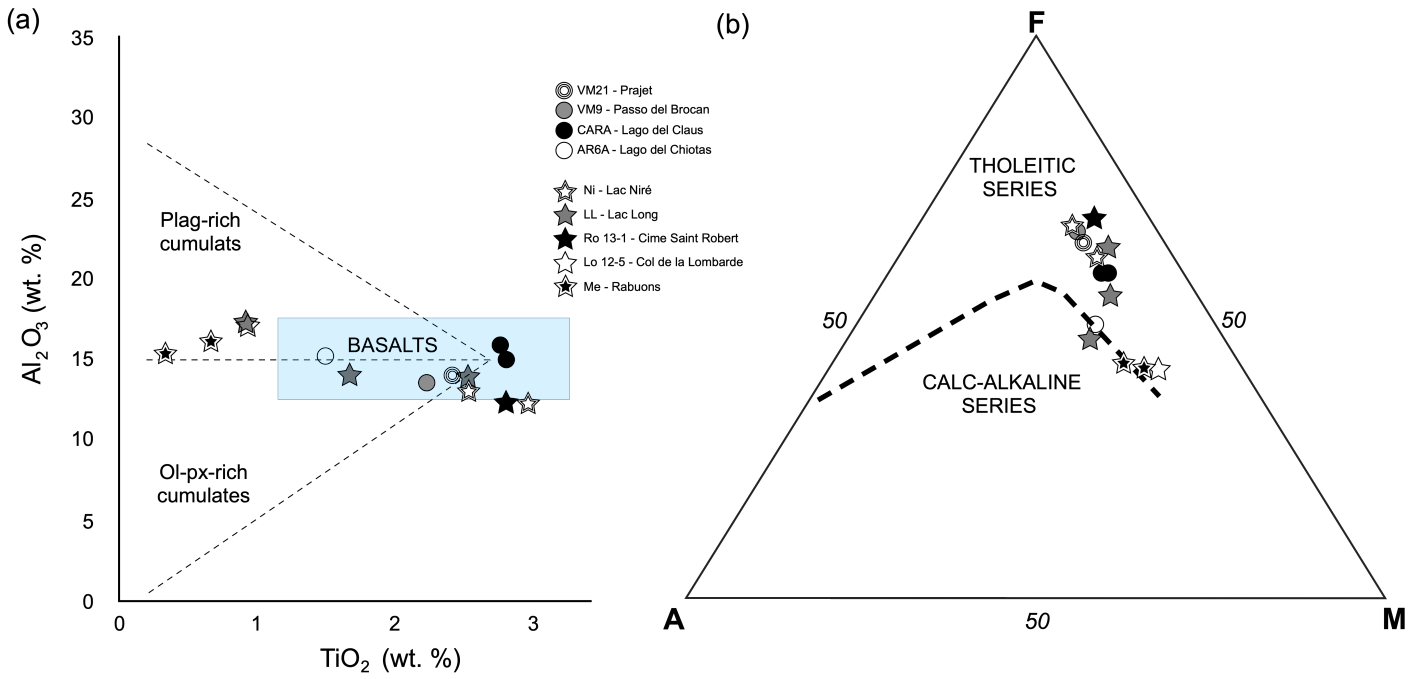
(a)
35
30
25
20
15
10
5
0
0
1
2
3
Al_2O_3 (wt. %)
TiO_2 (wt. %)
Plag-rich cumulats
Ol-px-rich cumulates
BASALTS
VM21 - Prajet
VM9 - Passo del Brocan
CARA - Lago del Claus
AR6A - Lago del Chiotas
Ni - Lac Niré
LL - Lac Long
Ro 13-1 - Cime Saint Robert
Lo 12-5 - Col de la Lombarde
Me - Rabuons
(b)
F
A
M
50
50
50
THOLEITIC SERIES
CALC-ALKALINE SERIES

FIGURE 7

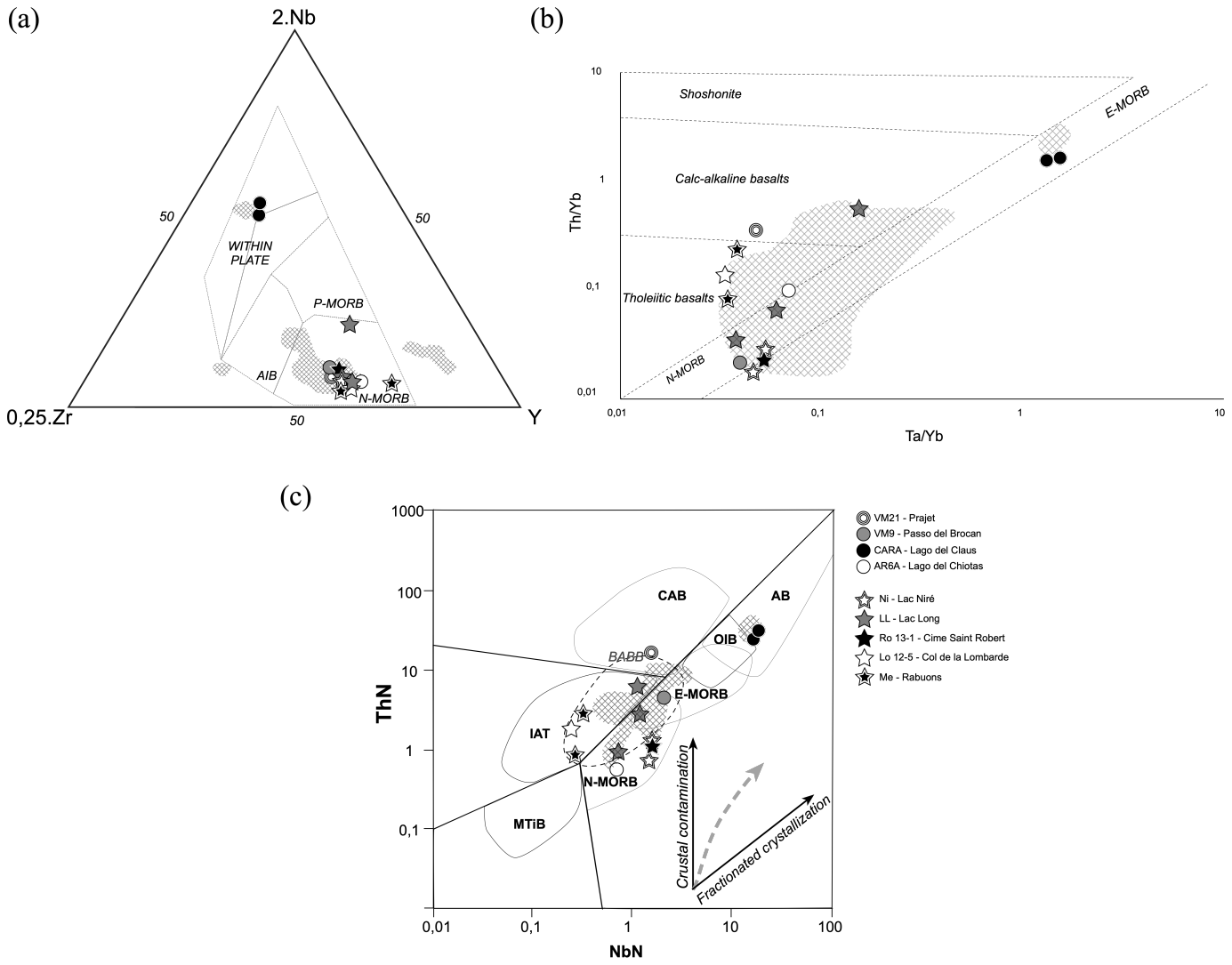
(a)
2.Nb
50
50
WITHIN PLATE
P-MORB
AIB
N-MORB
0,25.Zr
50
Y
(b)
Shoshonite
E-MORB
Calc-alkaline basalts
Tholeiitic basalts
N-MORB
Th/Yb
Ta/Yb
10
1
0,1
0,01
0,01
0,1
1
10
(c)
CAB
AB
OIB
BABB
E-MORB
IAT
N-MORB
MTiB
Crustal contamination
Fractionated crystallization
ThN
NbN
1000
100
10
1
0,1
0,01
0,1
1
10
100
VM21 - Prajet
VM9 - Passo del Brocan
CARA - Lago del Claus
AR6A - Lago del Chiotas
Ni - Lac Niré
LL - Lac Long
Ro 13-1 - Cime Saint Robert
Lo 12-5 - Col de la Lombarde
Me - Rabuons

FIGURE 8

(a)

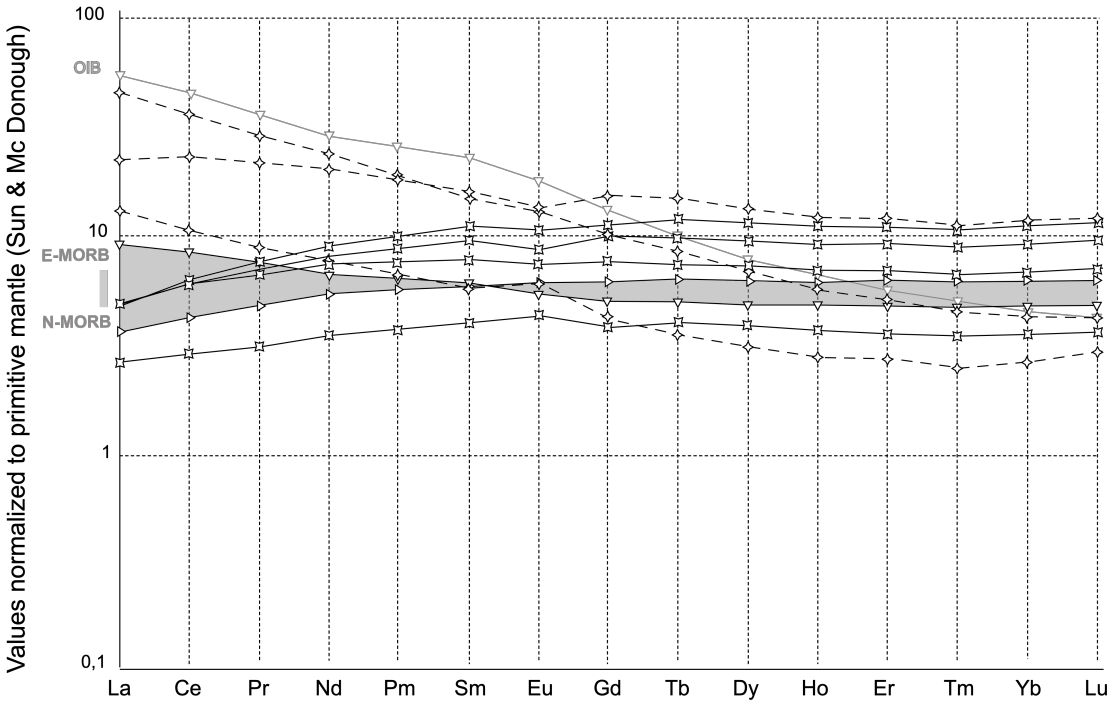
Values normalized to primitive mantle (Sun & Mc Donough)
100
OIB
10
E-MORB
N-MORB
1
0,1
La
Ce
Pr
Nd
Pm
Sm
Eu
Gd
Tb
Dy
Ho
Er
Tm
Yb
Lu

(b)

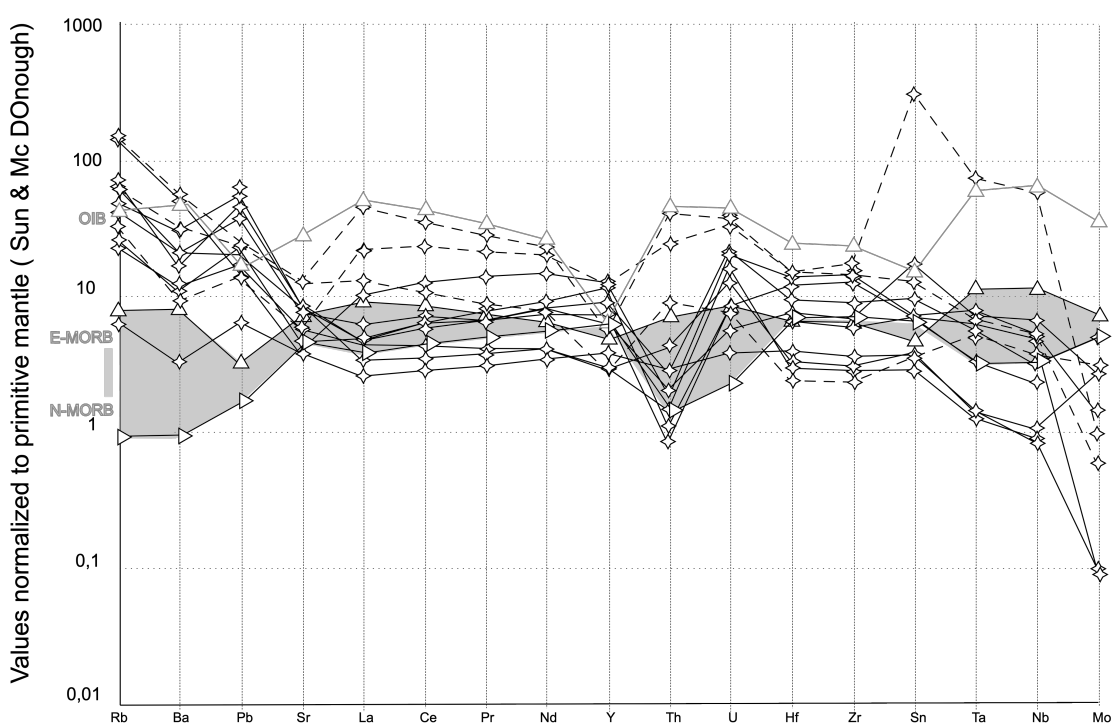
Values normalized to primitive mantle (Sun & Mc DOnough)
1000
100
OIB
10
E-MORB
N-MORB
1
0,1
0,01
Rb
Ba
Pb
Sr
La
Ce
Pr
Nd
Y
Th
U
Hf
Zr
Sn
Ta
Nb
Mo

FIGURE 9

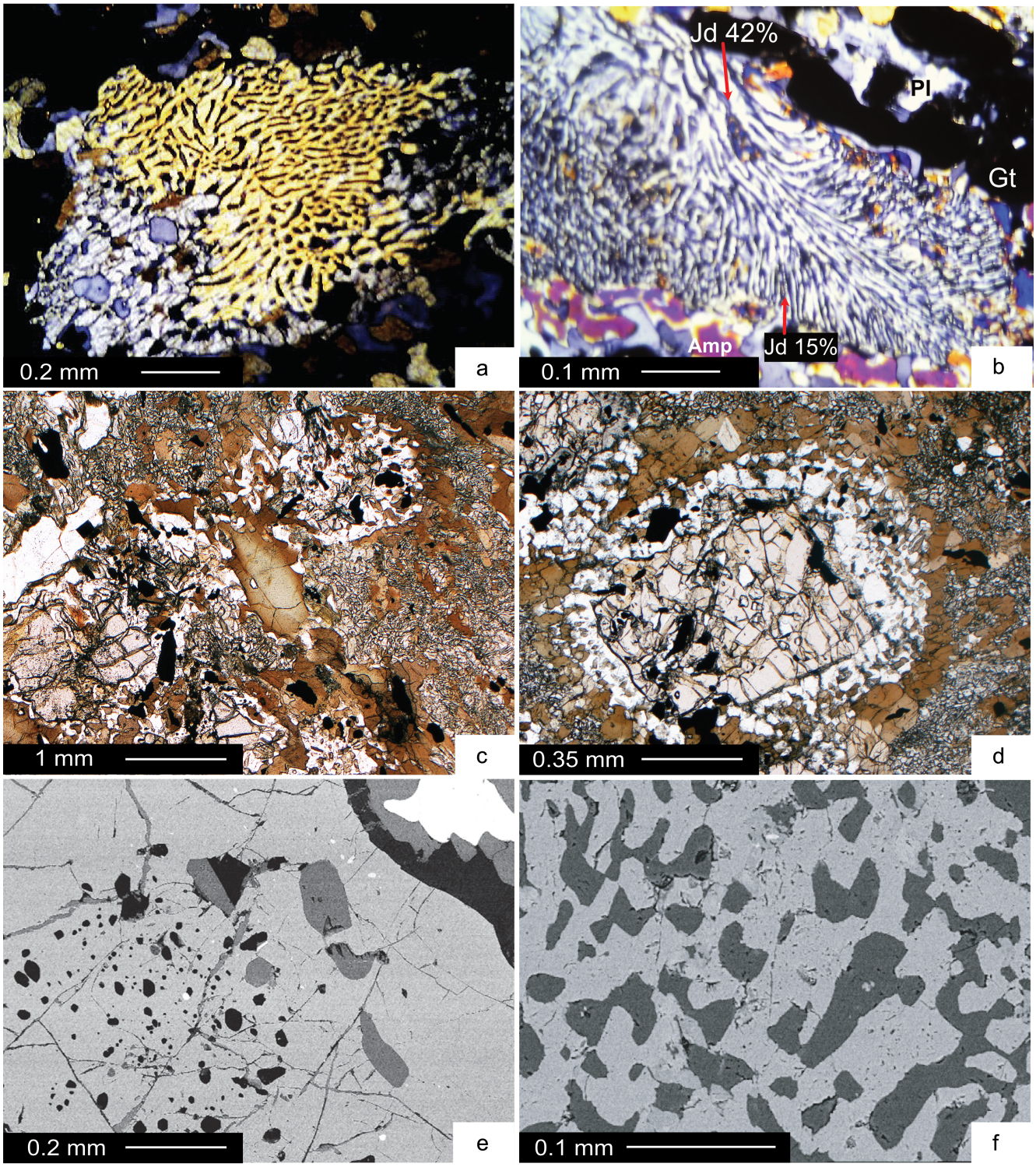

FIGURE 10

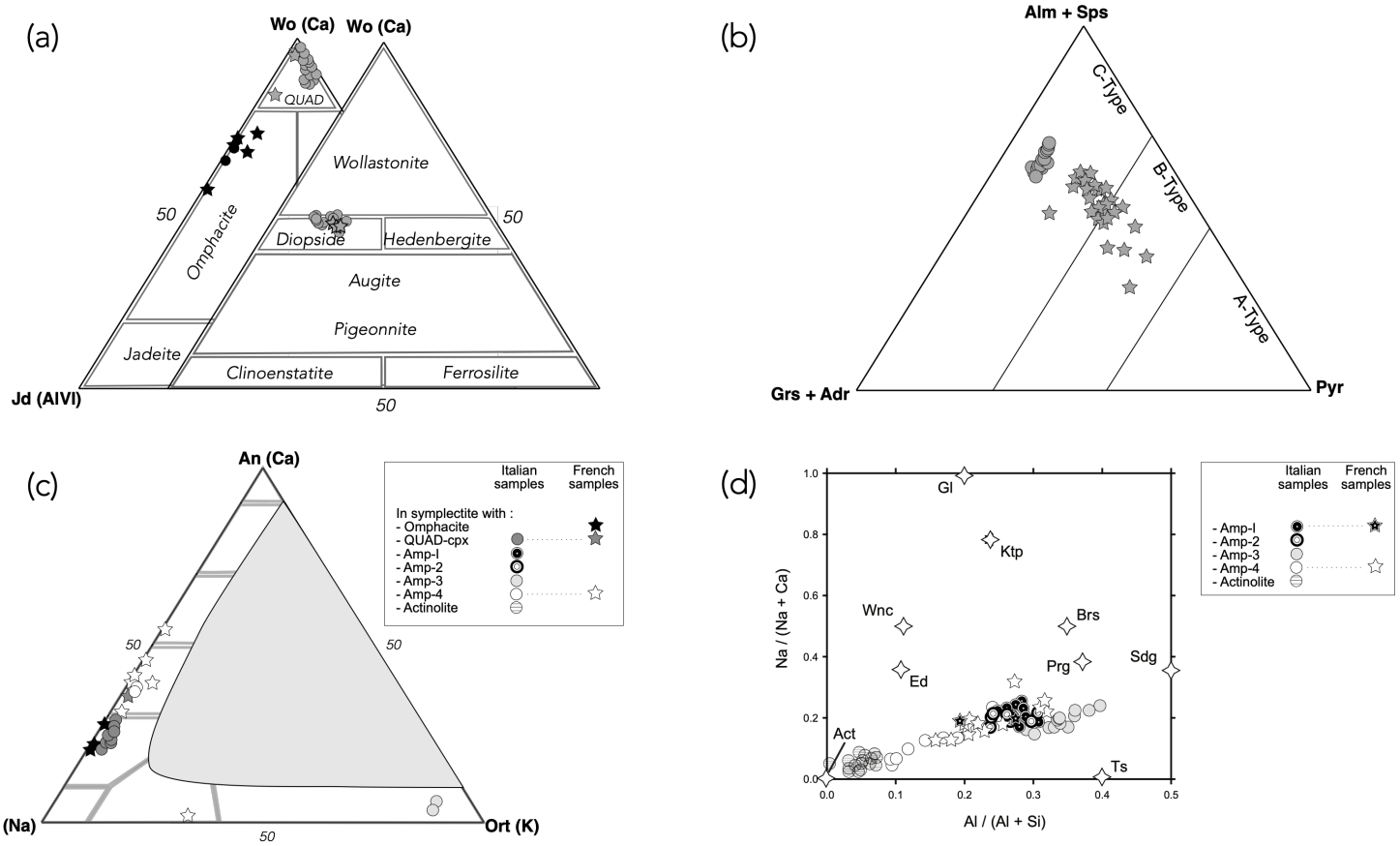
(a)
Wo (Ca)
Wo (Ca)
QUAD
Wollastonite
50
Omphacite
50
Diopside
Hedenbergite
Augite
Pigeonnite
Jadeite
Clinoenstatite
Ferrosilite
Jd (AlVI)
50
(b)
Alm + Sps
C-Type
B-Type
A-Type
Grs + Adr
Pyr
(c)
An (Ca)
Italian samples
French samples
In symplectite with :
- Omphacite
- QUAD-cpx
- Amp-I
- Amp-2
- Amp-3
- Amp-4
- Actinolite
50
50
Al (Na)
50
Ort (K)
(d)
Gl
Ktp
Wnc
Brs
Sdg
Prg
Ed
Act
Ts
Na / (Na + Ca)
Al / (Al + Si)
Italian samples
French samples
- Amp-I
- Amp-2
- Amp-3
- Amp-4
- Actinolite

FIGURE 11

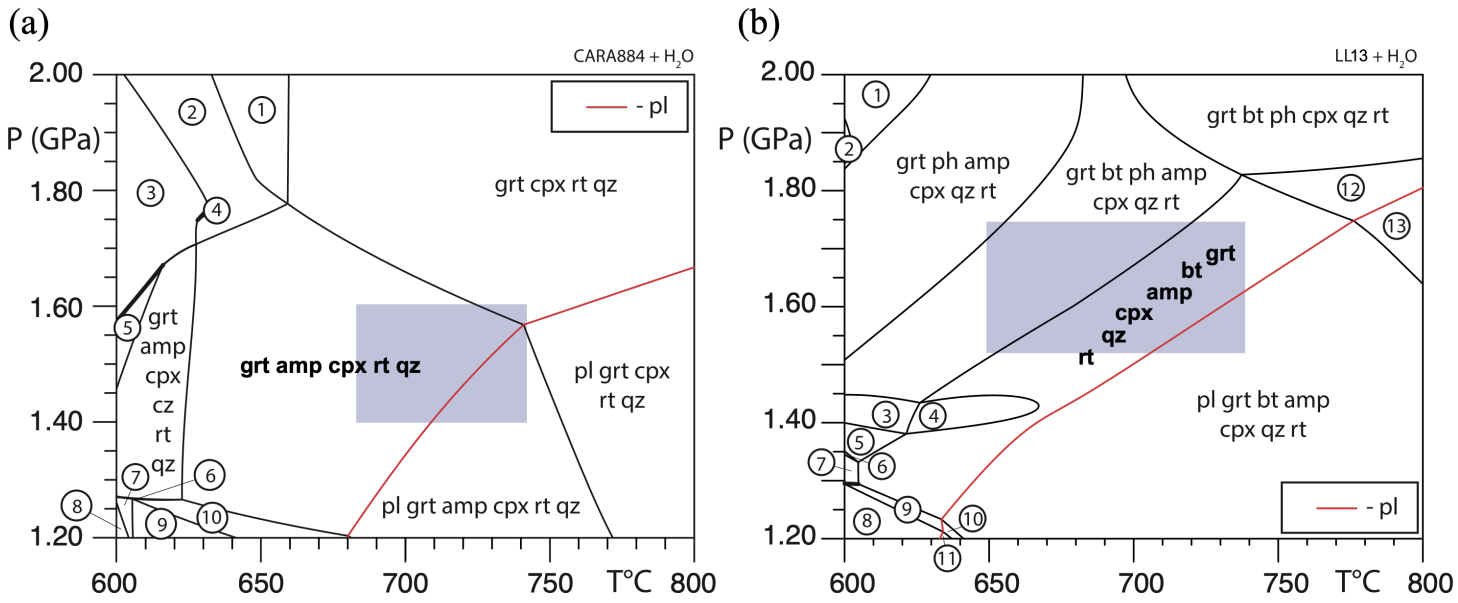
(a)
CARA884 + H2O
2.00
1.80
1.60
1.40
1.20
P (GPa)
600
650
700
750
T°C
800
- pl
grt cpx rt qz
grt amp cpx rt qz
pl grt cpx rt qz
pl grt amp cpx rt qz
grt amp cpx cz rt qz
(b)
LL13 + H2O
grt ph amp cpx qz rt
grt bt ph amp cpx qz rt
grt bt ph cpx qz rt
grt bt amp cpx qz rt
grt bt amp cpx qz rt
- pl

FIGURE 12

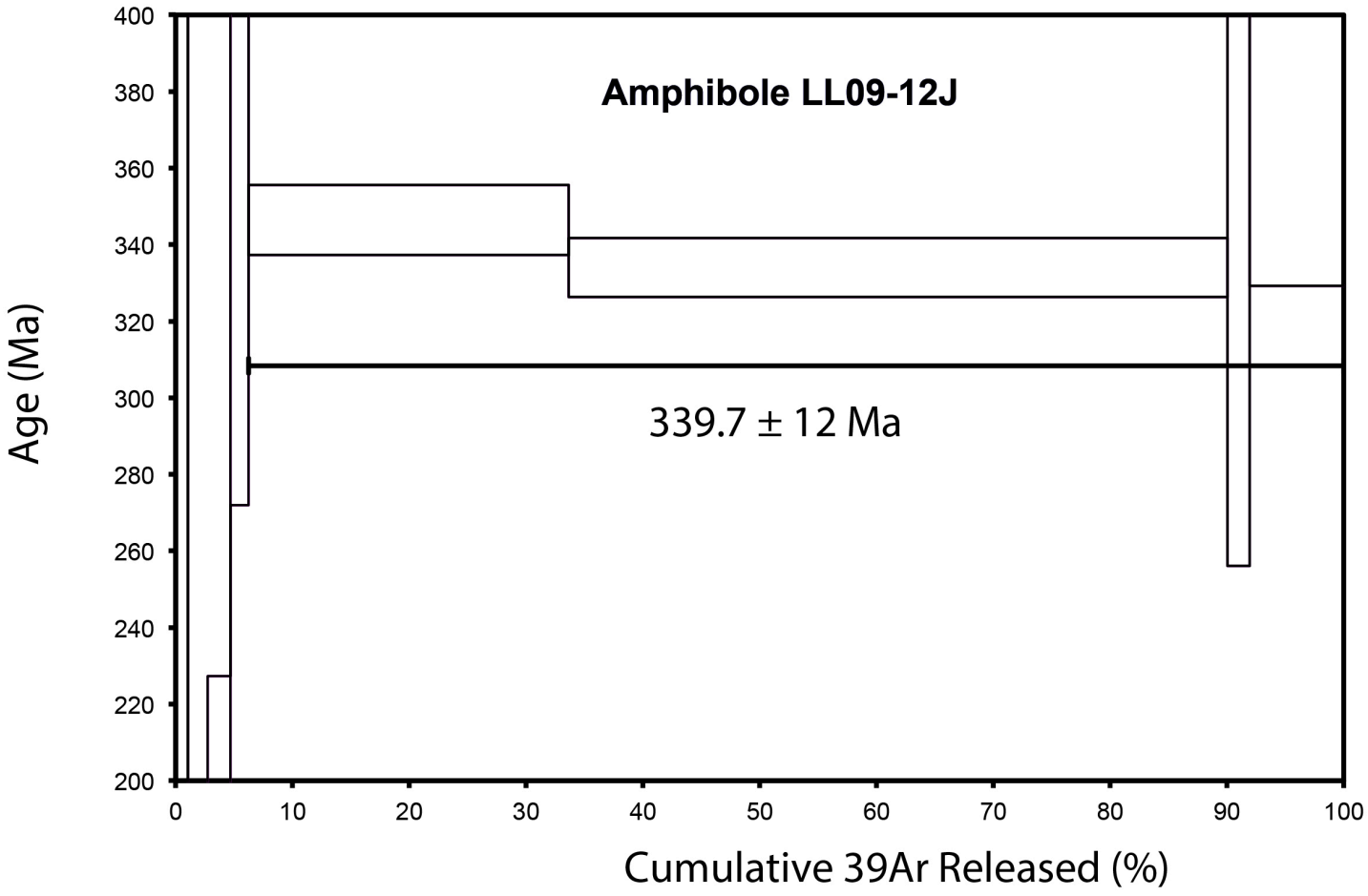
Amphibole LL09-12J
339.7 ± 12 Ma
Age (Ma)
Cumulative 39Ar Released (%)
400
380
360
340
320
300
280
260
240
220
200
0
10
20
30
40
50
60
70
80
90
100

FIGURE 13

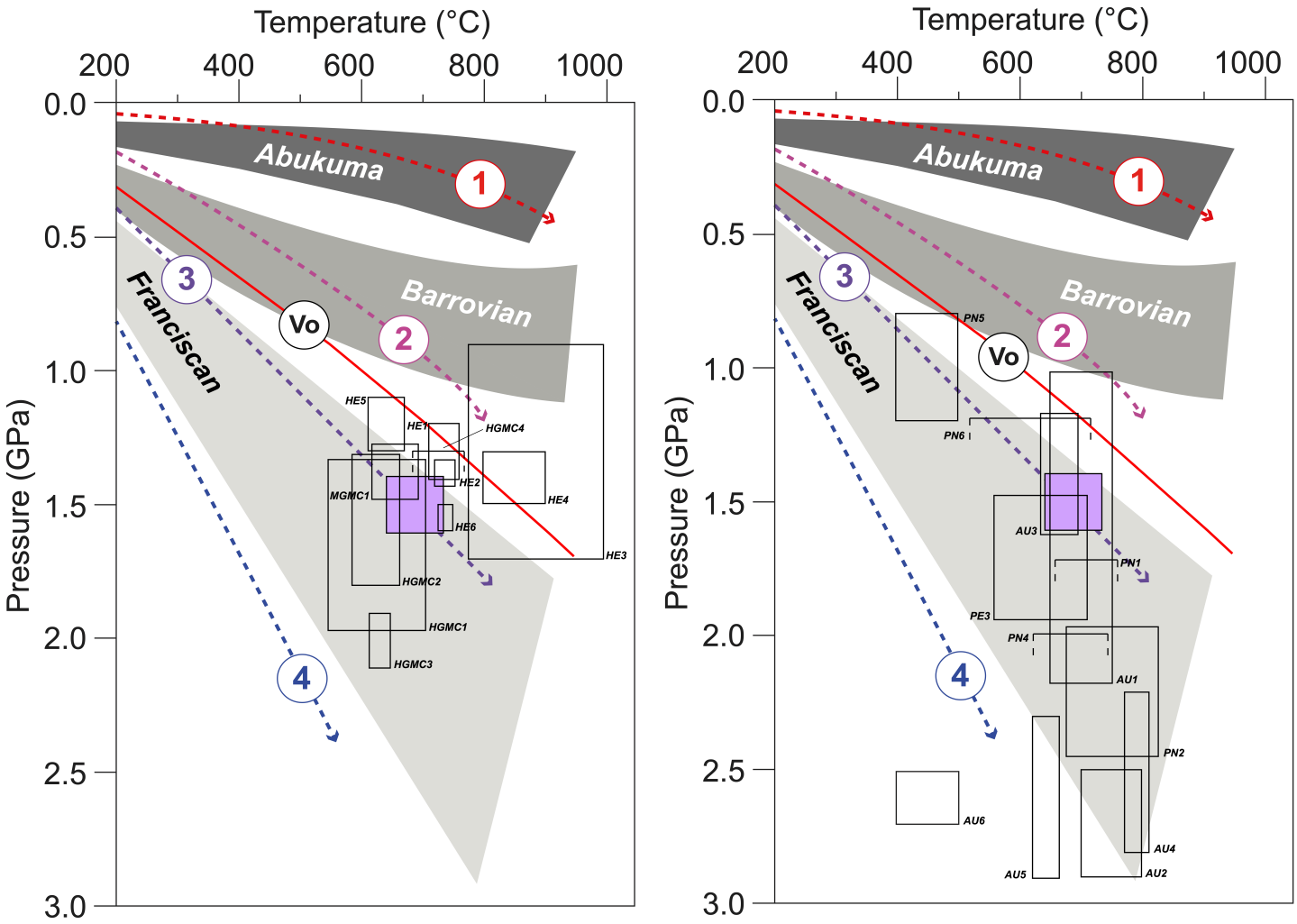
Temperature (°C)
200
400
600
800
1000
0.0
0.5
1.0
1.5
2.0
2.5
3.0
Pressure (GPa)
Abukuma
Barrovian
Franciscan
Vo
1
2
3
4
HE5
HE1
HGMC4
HE2
HE4
MGMC1
HE6
HE3
HGMC2
HGMC1
HGMC3
PN5
PN6
AU3
PN1
PE3
PN4
AU1
PN2
AU6
AU4
AU5
AU2

FIGURE 14